Chaos, Solitons and Fractals 192 (2025) 116037

Contents lists available at ScienceDirect

Chaos, Solitons and Fractals

journal homepage: www.elsevier.com/locate/chaos

Global bifurcation in a virus, defective genomes, satellite RNAs tripartite system: Breakdown of a coexistence quasi-neutral curve

Oriol Llopis-Almela [a,*], J. Tomás Lázaro [a,b,c,d], Santiago F. Elena [e,f], Josep Sardanyés [a,d,**]

[a] Centre de Recerca Matemàtica (CRM). Campus de Bellaterra. Edifici C, Cerdanyola del Vallès, 08193 Barcelona, Spain
[b] Departament de Matemàtiques. Universitat Politècnica de Catalunya (UPC), Avda. Diagonal 647, 08028 Barcelona, Spain
[c] Institute of Mathematics of the UPC-BarcelonaTech (IMTech), C. Pau Gargallo 14, 08028 Barcelona, Spain
[d] Dynamical Systems and Computational Virology. CSIC Associated Unit CRM-I^{2}SysBio, Spain
[e] Institute for Integrative Systems Biology (I^{2}SysBio). CSIC-Universitat de València, Avda. Catedrático Agustín Escardino Benlloch 9, Paterna, 46980 València, Spain
[f] The Santa Fe Institute, 1399 Hyde Park Road, Santa Fe, NM 87501, USA

ARTICLE INFO

Keywords:
Bifurcations
Complex systems
Defective interfering genomes
Dynamical systems
Satellite RNAs
Subviral particles

ABSTRACT

The dynamics of wild-type (wt) RNA viruses and their defective viral genomes (DVGs) have been extensively studied both experimentally and theoretically. This research has paid special attention to the interference effects of DVGs on wt accumulation, transmission, disease severity, and induction of immunological responses. This subject is currently a highly active and promising area of research since engineered versions of DVGs have been shown to act as antiviral agents. However, viral infections involving wt, DVGs, and other subviral genetic elements, like viral RNA satellites (satRNAs), have received scarce attention. Satellites are molecular parasites genetically different from the wt virus, which exploit the products of the latter for their own replication in as much as DVGs do, and thus they need to coinfect host cells along with the wt virus to complete their replication cycle. Despite satRNAs being very common, their dynamics co-infecting with wt viruses have been poorly investigated. Here, we analyze a mathematical model describing the initial replication phase of a wt virus producing DVGs and coinfecting with a satRNA. The model, which explicitly considers the viral RNA-dependent RNA polymerase produced by the wt virus, has three different dynamical regimes depending upon the wt replication rate (α), the fraction of DVGs produced during replication (ω), and the replication rate of the satRNA (β): (*i*) full extinction when $\beta > \alpha(1-\omega)$; (*ii*) a bistable regime with full coexistence governed by a quasi-neutral curve of equilibria and full extinction when $\beta = \alpha(1-\omega)$; and (*iii*) a scenario of bistability separating full extinction from wt-DVGs coexistence with no satRNA when $\beta < \alpha(1-\omega)$. The transition from scenarios (*i*) to (*iii*) occurs through the creation and destruction of a quasi-neutral curve of equilibria in a global bifurcation that we name as *quasi-neutral nullcline confluence* (QNC) bifurcation: at the bifurcation value, two nullcline hypersurfaces coincide, giving rise to the curve of equilibria. In agreement with previous research on global bifurcations tied to quasi-neutral manifolds, we have identified numerically and derived analytically scaling laws of the form $\tau \sim |\mu|^{-1}$, with τ being the length of the transients close to the remnant curve and μ the distance to the bifurcation value.

1. Introduction

The interaction amongst full-genome wild-type (wt) viruses and the plethora of non-standard viral genomes (nsVGs) that may coexist within the same infected host cell is essential to forecast the outcome of infections and their impact on virulence. Viruses infect cells and unfold their replication mechanisms to carry out a complete infectious cycle by kidnapping host cells' resources. This property turns them into obligate intracellular parasites for their replication and further propagation [1]. Particularly, RNA viruses are characterized by extremely large population sizes and very fast rates of evolution [2]. This is due to the high mutation rates, since the viral-encoded RNA-dependent RNA polymerase (RdRp) generically lacks a proofreading mechanism [3,4]. Broadly speaking, nsVGs can be classified into two groups [5], (*i*) those that are generated by erroneous replication of the wt genome by the

* Corresponding author.
** Corresponding author at: Centre de Recerca Matemàtica (CRM). Campus de Bellaterra. Edifici C, Cerdanyola del Vallès, 08193 Barcelona, Spain.
E-mail addresses: ollopis@crm.cat (O. Llopis-Almela), jose.tomas.lazaro@upc.edu (J.T. Lázaro), santiago.elena@csic.es (S.F. Elena), jsardanyes@crm.cat (J. Sardanyés).

https://doi.org/10.1016/j.chaos.2025.116037
Received 30 October 2024; Received in revised form 5 January 2025; Accepted 14 January 2025

viral RdRp and include hypermutated genomes, deletions, insertions, and different types of reorganized genomes, collectively known as defective viral genomes (DVGs); and (*ii*) other RNA genomes that are not genetically related to the wt virus but coinfect with it and could encode (satellite viruses) or not (satellite RNAs—satRNAs) their own proteins. In common, all these nsVGs are unable to complete a replication cycle in the absence of a wt virus that acts as a helper (HV) that provides all the necessary factors [6]. Among the diverse types of DVGs, some can disrupt viral replication by hijacking proteins encoded by the wt virus. This specific type of DVGs, called defective interfering particles (DIPs), was first identified by Huang and Baltimore in the 1970s [7].

Coinfections or superinfections[1] of the HV with other subviral genetic elements, such as satellite viruses and satRNAs, can have a big impact on virus dynamics and modulate symptomatology. Satellites are usually non-related genetically to the HV [8], but they depend on it for replication, infection, and/or movement, as DIPs do. Satellites can influence viral pathogenicity and accumulation. Unlike satRNAs, satellite viruses contain genetic instructions to, *e.g.*, produce a protein to encapsulate their genomes. Virus satellites and satRNAs are very common in plant infections [9,10], and some satellites are known to infect unicellular eukaryotic cells [11], insects [12], and vertebrates [13]. The implications of satellites in ongoing infections cover a wide range of symptoms: from attenuation, for instance, due to a decrease of RNA HV accumulation [14], to symptoms aggravation [15], as it is the case for broad bean mottle virus and turnip crinkle virus [9,10], or for the hepatitis delta virus (HDV). HDV is a virus satellite that infects together with the hepatitis B virus (HBV), using the HBV surface antigen to form enveloped particles capable of cell-to-cell transmission [16]. However, it is able to replicate in the absence of HBV since its replication is mediated by the host cell DNA-dependent RNA polymerases [17]. HDV coinfection with HBV or superinfection of HBV carriers often results in exacerbation of the underlying HBV hepatitis [18], giving rise to more damaging liver disease and a more rapid evolution towards hepatocellular carcinoma. The prevalence of HDV among HBV carriers is 13.02%, corresponding to 48–60 million infections globally [19].

Despite the large number of examples of viral coinfections with satellites, the dynamics of these systems formed by hyperparasites (nsVGs) of parasites (HV) have been poorly studied, especially from a dynamical perspective. In this article we investigate a mathematical model describing the initial phase of the within-cell replication process of an RNA HV producing DVGs that act as DIPs and coinfecting with a satRNA. Previous research explored a similar system considering these three parasitic agents [20]. Our model, as a difference from the one presented in [20], explicitly includes the dynamics of the RdRp, whose production depends on the amount of HV and supports the replication of the three RNA molecular species, also introducing further nonlinearities into the system. The viral genome for positive-sense single-stranded RNAs acts as a messenger RNA. Once it enters into the host cell, it is directly translated by the cell ribosomes to produce the RdRp and other early proteins [21]. RdRp will then bind the genomic RNA and generate the HV and nsVGs progenies. The studied model shows parameter conditions for which the phase space exhibits a quasi-neutral curve made up of equilibrium points allowing the coexistence of the HV and the two subviral elements.

In dynamical systems, a quasi-neutral manifold refers to a set of equilibrium points that form a continuous manifold, rather than isolated equilibria. Such a continuum of equilibria leads to the appearance of zero eigenvalues of the linearized system around them and to the existence of an associated center manifold. Under this setting, different initial conditions typically achieve different equilibrium values. Quasi-neutral manifolds have been previously described in dynamical models for viruses, including asymmetric RNA replication modes [22] and epidemiological-like models investigating betacoronaviruses infections in cell cultures. For this latter system, dynamics were multi-stable and governed by quasi-neutral planes filled with equilibria [23]. Quasi-neutral manifolds have also been found in nonlinear systems describing the dynamics of allele fixation [24,25], in models of sexual diploid populations [26,27], in host-parasite systems [28], in a two-species Lotka–Volterra model [29], and in predator–prey dynamical systems displaying quasi-neutral surfaces [30]. Quasi-neutral curves of equilibria are invariant and uniparametric mathematical objects consisting of a continuum of equilibrium points with local attracting or repelling directions together with neutral ones [31]. They can play an essential role in organizing the global dynamics of a dynamical system to the extent that they can stand for the boundary between two qualitatively different regimes. That is to say, basins of attraction of different equilibrium points may change drastically in a neighborhood of the parameter value for which the quasi-neutral curve exists as well as the topological structure of the phase portrait [28]. Here, we describe a global bifurcation tied to this quasi-neutral curve that we have named as the *quasi-neutral nullcline confluence* (QNC) bifurcation. This bifurcation involves the creation and destruction of a curve of equilibrium points that arises for specific parameter conditions, making two three-dimensional nullclines coincide. This phenomenon of loss of stability inside a line of equilibria by means of a real eigenvalue changing sign was already described by Fiedler, Liebscher, and Alexander in [32, Theorems 1.1 and 1.2] and by Fiedler and Liebscher in [33]. In these works a C^1 local conjugacy to a suitable normal was provided. The counterpart case, where this loss of stability follows from a generic Hopf bifurcation, was also treated by the same authors in [32] and related papers. Other similar global bifurcations have been described in lower dimensions by Fontich and colleagues [28]. For an interesting example of the use of topological techniques, based on Conley Index Theory, to investigate invariant structures and global connections among equilibria, we refer the reader to [34].

Our investigation focuses on the dynamics in a neighborhood of these parameter conditions, in which nearby orbits passing close to a remnant of the (non-existing) quasi-neutral curve remain for a long time close to it, experiencing a kind of ghost effect that largely delays the orbits. Ghosts and bottlenecks causing a slowing down of dynamics have been widely studied for local bifurcations [35–38]. More recently, this concept has been generalized by the so-called ghost channels and ghost cycles. The implications of these ghost structures have been discussed in the context of stability and stochastic dynamics [39].

The manuscript is organized as follows. In Section 2 we introduce the mathematical model describing the dynamics of complementation and competition of a tripartite system composed of a wt virus producing DIPs under the presence of a satRNA. Section 3 contains the investigation of the dynamics' domain, nullclines, and invariant sets. Here, the equilibrium points and some global aspects of the dynamics are inspected. Then, we focus on the geometry and the dynamics tied to the quasi-neutral curve of equilibria. We also analyze a global bifurcation involving the disappearance of this quasi-neutral curve, and we describe a new mechanism of slowing down tied to the remnant of this curve (a kind of ghost channel). This slowing down is shown to be governed by scaling laws with exponent -1 with respect to a close distance between the bifurcation parameter before and after the bifurcation value. Some conclusions about the possible roles of these dynamics in early viral infections are finally outlined in Section 4. In order to ease the reading, the proofs of all the relevant results presented in all sections are provided in Appendices A and B. In some cases, if the proof is straightforward, it has been omitted.

2. Mathematical model

Let us define $x = (V, S, D)$ as the vector of state variables containing the population densities of the three RNA species: the HV (V), the

[1] Coinfection refers to two different viral types entering the cell at the same time. Superinfection refers to the subsequent infection of a host already infected by another viral type.

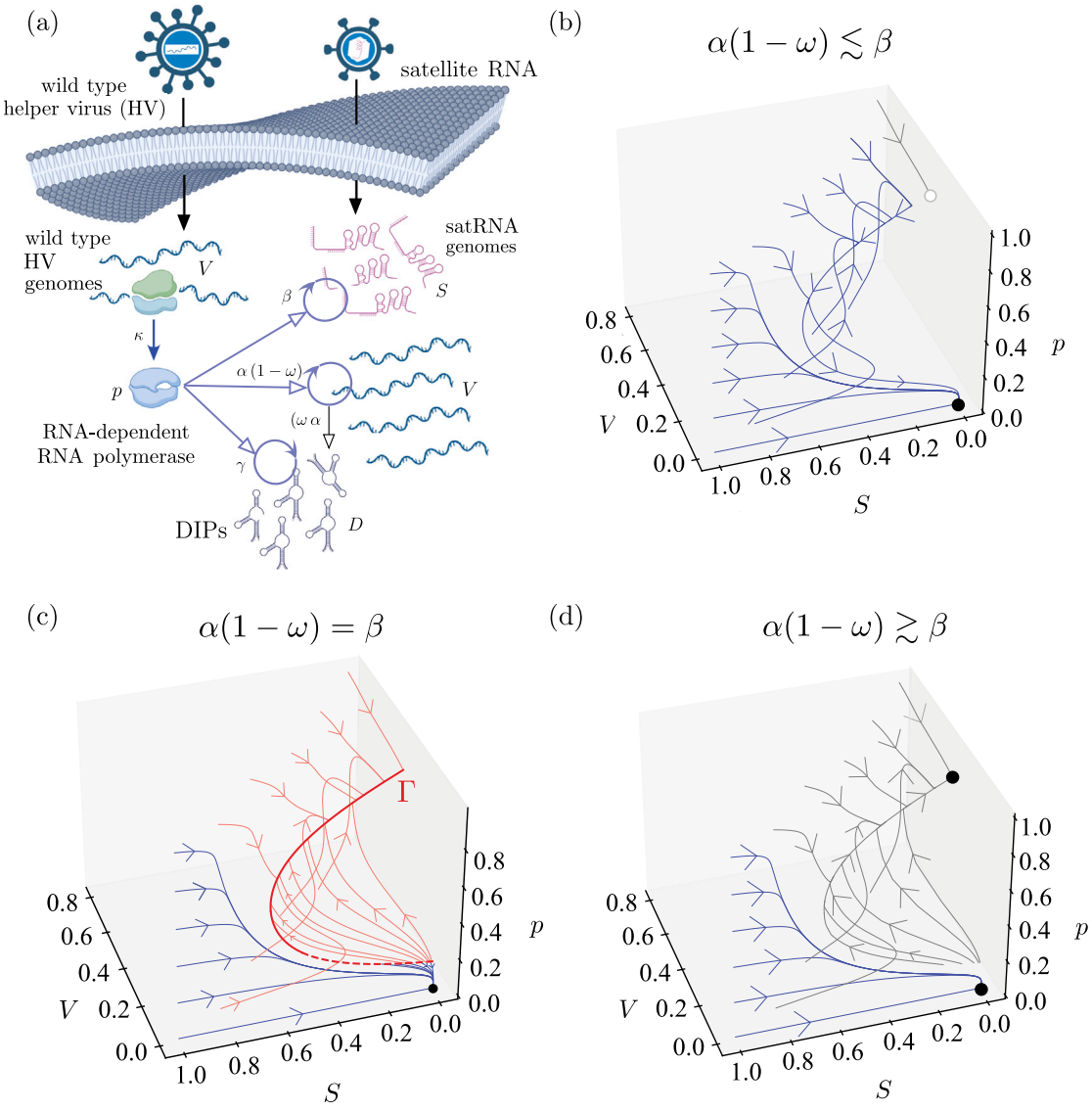

Fig. 1. (a) Schematic diagram of the main interactions modeled for the tripartite system wild-type helper virus (HV), its interfering defective particles (DIPs), and a satellite RNA (satRNA) coinfecting the same cell. The HV RNA genome is translated into the viral RNA-dependent RNA polymerase (RdRp) at a constant rate κ. The RdRp replicates the HV genomes, which produce DIPs at a rate $\alpha\omega$, being ω the fraction of DIPs produced by mutation during replication, and thus $1-\omega$ being the fraction of error-free replication. The RdRp also supports the replication of the DIPs (at a rate γ) and of the satRNAs (at a rate β). All the viral agents compete for cellular resources such as nucleotides. Panels (b-d) display phase portraits for three qualitatively different scenarios which depend on the effective replication rate of the HV, $\alpha(1-\omega)$, and the replication rate of the satRNA β. The values of the parameters used to compute numerically the orbits in (b-d) are given by $\beta = 0.7$, $\omega = 0.2$, $\gamma = 0.6$, $\kappa = 0.3$, $\varepsilon = 0.1$ and $\varepsilon_p = 0.01$; with (b) $\alpha = 0.874999$, (c) $\alpha = 0.875$, and (d) $\alpha = 0.875001$. The quasi-neutral curve Γ is displayed in (c) with a red curve with locally stable (solid line) and unstable (dashed line) branches. The black dots denote local asymptotically stable equilibrium points. White dots are equilibrium points of saddle type with three-dimensional stable manifolds and an unstable one. Blue orbits belong to the basin of attraction of the origin Q_0; gray orbits to the basin of attraction of the satRNA-extinction equilibrium point Q_1, and the red ones to the basin of attraction of coexistence equilibria Q_2. (For interpretation of the references to color in this figure legend, the reader is referred to the web version of this article.)

DVGs (D), and the satRNAs (S). Let us also consider the viral RdRp (p), encoded by the HV and supporting the replication of the three RNA species, as another state variable. The within-cell dynamics for this system [schematized in Fig. 1(a)] can be described by the following system of autonomous ordinary differential equations:

$$\dot{V} = \alpha(1-\omega)\, V\, p\, \Omega(x) - \varepsilon\, V, \tag{1}$$

$$\dot{S} = \beta\, S\, p\, \Omega(x) - \varepsilon\, S, \tag{2}$$

$$\dot{D} = (\omega\alpha\, V + \gamma\, D)\, p\, \Omega(x) - \varepsilon\, D, \tag{3}$$

$$\dot{p} = \kappa\, V \left(1 - \frac{p}{C_1}\right) - \varepsilon_p\, p, \tag{4}$$

with

$$\Omega(x) = 1 - \left(\frac{V+S+D}{C_0}\right).$$

The model considers the processes of RdRp translation, genomes' replication, production of DVGs, competition, complementation, and RNA degradation. Concerning the viral RdRp, its dynamic equation describes the processes of enzyme production and degradation. Here we assume that the production of the RdRp is limited by finite resources, *e.g.*, available ribosomes, tRNAs, amino acids, and/or other cellular cofactors and we model it with the logistic term $(1 - p/C_1)$, setting the carrying capacity for the proteins to $C_1 = 1$ for simplicity. The other logistic-like term $\Omega(x)$, also using a normalized carrying capacity ($C_0 = 1$) to simplify the calculations, introduces intra- and inter-specific competition between the viral RNAs. Such a competition is assumed also occur due to cellular finite resources, *i.e.*, nucleotide triphosphates, ATP, membranes, and other cellular and/or viral cofactors. For simplicity, we focus on the initial replication stages without modeling the encapsidation and formation of virions.

The model parameters are given by the replication rates of the HV ($\alpha > 0$), the satRNA ($\beta > 0$), and the DIPs ($\gamma > 0$). Despite the replication rates for the DIPs and the satRNA being expected to be faster than the one of the HV, owing to differences in genome length (see Tables 1 − 5 in [10] for genome lengths of satRNAs), we will provide a general investigation of these parameters. The replication speed of each of the RNA species will certainly depend on the length of their genomes, but other factors can also influence these relative replication rates. These can include the secondary structures of viral RNAs *e.g.*, stem-loops can act as physical barriers slowing down the RdRp advance over the RNA template molecule and require unwinding [40]. Related to this unwinding process, the availability of helicases can also be of importance in facilitating replication [41], as well as nucleotide triphosphate availability [42]. Moreover, host proteins such as heteronuclear ribonucleoproteins (hnRNPs) can influence replication speed, either facilitating or inhibiting replication [43], or the capability of RNAs to access the replication factories associated with the endoplasmic reticulum [44]. Moreover, by investigating the dynamics for arbitrary parameter values within the biological ballpark, it may be possible to adapt these values for specific viruses, particularly in relation to the synthesis rates of new genomes. The model also considers that the HV produces a fraction $\omega \in (0, 1]$ of DIPs due to errors during the process of HV transcription. In addition, we consider that the RdRp is produced proportionally to the amount of HV in a meaningful range value at a constant translation rate $\kappa > 0$. As mentioned above, here we are limiting the production of the RdRp with a logistic function also considering a normalized carrying capacity. Finally, the three RNA species are assumed to degrade spontaneously at a constant rate $\varepsilon > 0$ while RdRp degrades at a rate $\varepsilon_p > 0$ [see Fig. 1(a)].

Generically, the timescales for the initial phases of within-cell infection dynamics of RNA viruses are on the order of minutes to hours [1]. Hence, the timescales of the dynamics of Eqs. (1)–(4) to be biologically-meaningful would correspond to minutes (min). That is, the rate constants α, ϵ, β, γ, κ, and ϵ_p have units of min^{-1}.

As we discuss below, the different dynamics of the modeled dynamical system have a strong dependence on the effective HV replication given by $\alpha(1-\omega)$, and on the replication rate of the satRNA β. This fact is illustrated in Fig. 1(b-d).

3. Results

We first carry out an analytical description of the vector field unfolded by Eqs. (1)–(4). To do so, we define the biologically meaningful domain of dynamics, the expression for the nullclines and some invariant subsets. Then, we present two main results outlining different conditions for the existence of equilibrium points different from the origin.

3.1. Dynamics domain, nullclines and invariant subsets

According to former considerations, the dynamics of our system are confined to the following set in $\mathbb{R}^4$:

$$\mathcal{U} = \left\{ (V, S, D, p) \in \mathbb{R}^4 \;\middle|\; V, D, S \geq 0; \quad 0 \leq p \leq 1 \quad \text{and} \quad V + D + S \leq 1 \right\}. \tag{5}$$

Indeed, $\mathcal{U}$ is positively invariant since the hyperplanes $V = 0$ and $S = 0$ are invariant subsets; when $p = 0$, we have $\dot{p} > 0$ and when $p = 1$, we have $\dot{p} < 0$; for $D = 0$, $\dot{D} > 0$ and at $\Omega(x) = 0$, $\dot{V} < 0$, $\dot{D} < 0$ and $\dot{S} < 0$ in such a way that the flow points inwards the domain from all its boundaries. In fact, $\mathcal{U}$ consists of the Cartesian product between a 3-dimensional tetrahedron spanned by the three RNA populations, with finite faces at the intersection of planes $V = 0$, $S = 0$, $D = 0$ and $V + S + D = 1$; and the finite and closed real interval $[0, 1]$, which is the domain of the state variable p.

The V-nullcline has two components given by the invariant set $V = 0$ and the hyperquadric with expression

$$H_1 : p\,\Omega(x) = \frac{\varepsilon}{\alpha(1-\omega)} \iff p(1 - V - D - S) = \frac{\varepsilon}{\alpha(1-\omega)}. \tag{6}$$

Nullcline $\dot{S} = 0$ also exhibits two components given by the invariant set $S = 0$ and the hyperquadric embedded in the 4th-dimensional space with the following expression:

$$H_2 : p\,\Omega(x) = \frac{\varepsilon}{\beta} \iff p(1 - V - D - S) = \frac{\varepsilon}{\beta}. \tag{7}$$

Dynamics in the invariant hyperplane $S = 0$ do not modify the general dynamics since the satRNA only depends on the amount of RdRp to persist excluding competition processes. The nullcline $\dot{D} = 0$ is the algebraic surface $(\omega\alpha V + \gamma D)p\Omega(x) = \varepsilon D$ and the nullcline $\dot{p} = 0$ is provided in the lemma below.

Lemma 1. *Let $Q^* = (V^*, S^*, D^*, p^*)$ be any equilibrium point of system (1)–(4). Then,*

$$p^* = p^*(V^*) = 1 - \frac{\varepsilon_p}{\kappa V^* + \varepsilon_p}, \tag{8}$$

which corresponds to nullcline $\dot{p} = 0$. It satisfies $0 < p^* < 1$ and, moreover, $p^* = 0$ if and only if $V^* = 0$.

Nullclines (6)–(7) are parallel hypersurfaces that only intersect when they coincide for $\alpha(1 - \omega) = \beta$. In order for both of them to intersect $\mathcal{U}$, conditions $\varepsilon \leq \alpha(1 - \omega)$ and $\varepsilon \leq \beta$ must be fulfilled, which are reasonable restrictions since degradation rates are assumed to be much lower than the effective replication rates[2] for viral particles. Previous quantitative research on single-stranded positive-sense RNA viruses has shown that genome replication rates are approximately one or two orders of magnitude higher than their degradation rates [45]. When both H_1 and H_2 intersect $\mathcal{U}$, and given their parallelism, the 4-dimensional space is divided into three different disjoint sets. Assuming $\varepsilon \neq 0$, the intersection of H_1 and H_2 with $p = 0$ and $1 = V + D + S$ is empty and only the intersection with $V = 0$, $S = 0$, $D = 0$, and $p = 1$ is nonempty.

The subsets $V = 0$ and $S = 0$ are invariant.

Indeed, without HV, the dynamics of the RdRp only exhibit exponential decay, and thus, the DIPs and the satRNAs go to extinction. On the other hand, the dynamics within $S = 0$ are governed by the existence of V-D-p coexistence equilibrium points. The invariability of $S = 0$ makes the dynamics in the absence of satRNA completely independent of those dynamics with the four variables. This behavior is biologically expected since satRNAs are parasites of the HV[3] and, therefore, removing them just results in fewer viral agents taking profit of the host cell resources (less competition) and the RdRp synthesized by the HV.

3.2. Equilibrium points and non-existence of periodic orbits

This section is devoted to describing the invariant sets for Eqs. (1)–(4). Specifically, it deals with the existence of equilibrium points and periodic orbits. The first result rules out the existence of periodic orbits and, consequently, the existence of limit cycles.

Proposition 1 (*Non-Existence of Periodic Orbits*)**.** *There are no T-periodic solutions of the system (1)–(4) for any $T > 0$ with initial conditions in $\mathcal{U}$.*

An analysis of the equilibrium points of the system (1)–(4) gives rise to the following results. First, two different conditions are given, ensuring that the equilibrium point is the origin, the full extinction of the populations.

Lemma 2. *Let $Q^* = (V^*, S^*, D^*, p^*)$ be an equilibrium point of the system (1)–(4) and $V^* = 0$. Then, necessarily, Q^* is $Q_0 = (0, 0, 0, 0)$.*

[2] By effective replication rate we mean the net replication rate of the HV, given by $\alpha(1 - \omega)$, resulting in the production of new HV RNAs.

[3] satRNAs are molecular hyperparasites of the HV, which is also a parasite.

Lemma 3. *Let $Q^* = (V^*, S^*, D^*, p^*)$ be an equilibrium point of the system (1)–(4) and $\alpha(1-\omega) = \gamma$. Then, necessarily, Q^* is the origin $Q_0 = (0,0,0,0)$.*

Hence, by Lemma 3, when the HV V and its DIPs D replicate at exactly the same effective rate, the only possible equilibrium point is the origin. The local stability for the origin is provided in the following result for all values of the parameters.

Lemma 4. *The origin Q_0 is always locally asymptotically stable for any parameter values.*

Let $Q^* = (V^*, S^*, D^*, p^*)$ be an equilibrium point of system (1)–(4). Let us assume now that $V^* \neq 0$ and seek other equilibrium points different from the origin. In particular, from the equation $\dot{S} = 0$ and assuming $\beta \neq 0$ one has

$$S^*\beta\left(p\Omega(x) - \frac{\varepsilon}{\beta}\right) = 0, \tag{9}$$

giving rise to two different cases: equilibrium points such that $S^* = 0$, denoted by Q_1 (satRNA extinction equilibrium points); and equilibrium points such that $S^* \neq 0$, denoted by Q_2 (coexistence equilibrium points). Propositions below identify the different parameter conditions that must hold for Q_1-equilibrium points (Proposition 2) and Q_2-equilibrium points (Proposition 3) to exist.

Proposition 2 (*SatRNA Extinction Equilibrium Points*)**.** *Let us denote by $Q_1 = (V_1, 0, D_1, p_1)$ a satellite-free equilibrium point of the system (1)–(4) (i.e., with $S_1 = 0$). Then, a necessary condition for Q_1 to exist is that*

$$\alpha(1-\omega) > \max\{\gamma, \varepsilon\}. \tag{10}$$

Let assume that condition (10) holds and let us define the quadratic polynomial $q(V) = T_2V^2 + T_1V + T_0$, with coefficients

$$T_2 = \frac{\varepsilon\kappa(\alpha-\gamma)}{\alpha(1-\omega)-\gamma}, \qquad T_1 = -\kappa\varepsilon\left(1 - \frac{\varepsilon}{\alpha(1-\omega)}\right), \qquad T_0 = \frac{\varepsilon_p\varepsilon^2}{\alpha(1-\omega)},$$

and discriminant $\Delta = T_1^2 - 4T_0T_2$. Then, provided that $V_1 + D_1 \leq 1$ and $0 \leq p_1 \leq 1$, there are at most two points $Q_1 = (V_1, 0, D_1, p_1) \in \mathcal{U}$, given by

$$q(V_1) = 0, \qquad p_1(V_1) = 1 - \frac{\varepsilon_p}{\kappa V_1 + \varepsilon_p}, \qquad D_1(V_1) = \frac{\alpha\omega}{\alpha(1-\omega)-\gamma}V_1 \tag{11}$$

which are equilibrium points of the system (1)–(4). These two points coincide when Δ vanishes.

Remark 1. From a biological point of view, condition (10) corresponds to the fact that the effective growth rate of the HV is larger than its own degradation and the intrinsic growth rate of the DIPs.

Proposition 3 (*Coexistence Equilibrium Points*)**.** *Let $Q_2 = (V_2, S_2, D_2, p_2)$ be an equilibrium point of the system (1)–(4) with $S_2 \neq 0$. From Lemma 2 we know that $V_2 \neq 0$. Then, necessarily, we must have*

$$\alpha(1-\omega) = \beta \qquad \text{and} \qquad \beta > \gamma. \tag{12}$$

Let us assume that conditions (12) hold. Thus, $Q_2 = (V_2, S_2, D_2, p_2)$ is a coexistence equilibrium point if it satisfies that

$$p_2 = p_2(V_2) = 1 - \frac{\varepsilon_p}{\kappa V_2 + \varepsilon_p}, \qquad D_2 = \frac{\beta\omega}{(\beta-\gamma)(1-\omega)}V_2, \tag{13}$$

and (V_2, S_2) belongs to the piece of the conic

$$q_2(V_2, S_2) = -\kappa\left(1 + \frac{\alpha\omega}{\beta-\gamma}\right)V_2^2 + \kappa\left(1 - S_2 - \frac{\varepsilon}{\beta}\right)V_2 - \frac{\varepsilon\varepsilon_p}{\beta} = 0 \tag{14}$$

that falls in $\mathring{\mathcal{U}}$.

The polynomial $q(V)$ in Proposition 2 is a multiple of the polynomial $q_2(V_2, 0)$ given by (14), as expected, if we take into account that $\alpha(1-\omega) = \beta$ in $q_2(V_2, S_2)$. Precisely $q(V) = -\varepsilon q_2(V_2, 0)$. Furthermore, if S_2 satisfies that

$$2\kappa\left(1 + \frac{\alpha\omega}{\beta-\gamma}\right)V_2 \neq \kappa\left(1 - S_2 - \frac{\varepsilon}{\beta}\right), \tag{15}$$

then we have that $V_2 = f(S_2)$ verifies $q_2(f(S_2), S_2) = 0$ where

$$f(S_2) = \frac{-\kappa\left(1 - S_2 - \frac{\varepsilon}{\beta}\right) \pm \sqrt{\kappa^2\left(1 - S_2 - \frac{\varepsilon}{\beta}\right)^2 - 4\kappa\left(1 + \frac{\alpha\omega}{\beta-\gamma}\right)\frac{\varepsilon\varepsilon_p}{\beta}}}{-2\kappa\left(1 + \frac{\alpha\omega}{\beta-\gamma}\right)}. \tag{16}$$

This explicit expression has been employed throughout this work in the numerical computation of the Q_2-equilibrium points.

Notice that conditions in (12) can be biologically interpreted as: (*a*) $\alpha(1-\omega) > \gamma$, the HV's effective growth rate is larger than the DIPs' intrinsic replication rate, (*b*) $\beta > \gamma$, that is, both the HV and the satRNAs must replicate at a higher effective rate than the DIPs.

The existence of equilibrium points Q_1 and Q_2 is then a consequence of the balance between the effective replication rate of the HV ($\alpha(1-\omega)$), the intrinsic replication rates of both the satRNA (β) and the DIPs (γ), and the degradation rates of the viral populations (ε). The satRNA extinction equilibrium Q_1 requires that HV replicates faster than the DIPs and faster than its own degradation. On the other hand, coexistence equilibria are possible only provided that the HV and satRNAs replicate at exactly the same pace and faster than DIPs.

3.3. Geometry and dynamics of the coexistence quasi-neutral curve

Let us denote by Γ the curve of equilibrium points Q_2 provided by Proposition 3. If nothing is explicitly said, we will reduce the study of such Γ to its projection on the space (V, S, D). Moreover, along this section, conditions (12) and $V \neq 0$ will always be assumed and, for the sake of simplicity, we will refer to the flow induced by the system (1)–(4) simply as *the flow*.

From its definition, it is clear that Γ is a piece of a hyperbola in $\mathcal{U}$ contained in the plane

$$\Pi_{DV}: \quad D = \frac{\beta\omega}{(\beta-\gamma)(1-\omega)}V \tag{17}$$

(see Fig. 3(a) for a geometrical representation). The following two propositions prove the invariance property for two specific subsets within $\mathcal{U}$, which is a crucial constraint for the dynamics of this case and which do not hold in the general parameter situation. Precisely, they show that the plane Π_{DV} and any plane with expression $S/V = C$, where $C \in \mathbb{R}^+$ is a constant value, are invariant by the dynamics of system (1)–(4). Consequently, the intersection of both planes is a straight line corresponding to an orbit of the system when it is projected on the (V, S, D)-space. The following propositions hold in the case $\alpha(1-\omega) = \beta$:

Proposition 4. *The plane Π_{DV} is invariant by the flow.*

Proposition 5. *The function S/V is a first integral of system (1)–(4), that is,*

$$\frac{S(t)}{V(t)} = \frac{S(0)}{V(0)} \qquad \forall t \geq 0.$$

The existence of the first integral S/V, together with the invariance of Π_{DV}, provides information on the geometry of the orbits when $\alpha(1-\omega) = \beta$. Indeed, in the (V, S, D)-space, any straight line σ that is the intersection of the two planes $S/V = c$ and Π_{VD} is also invariant by the flow: given any initial condition on σ, the corresponding orbit stays in σ for $t \in \mathbb{R}$ and, actually, σ itself is an orbit of the system. Since Γ is a branch of a hyperbola contained in Π_{DV}, any line σ must intersect it in two points, one point, or none. Let us assume that it does so in two

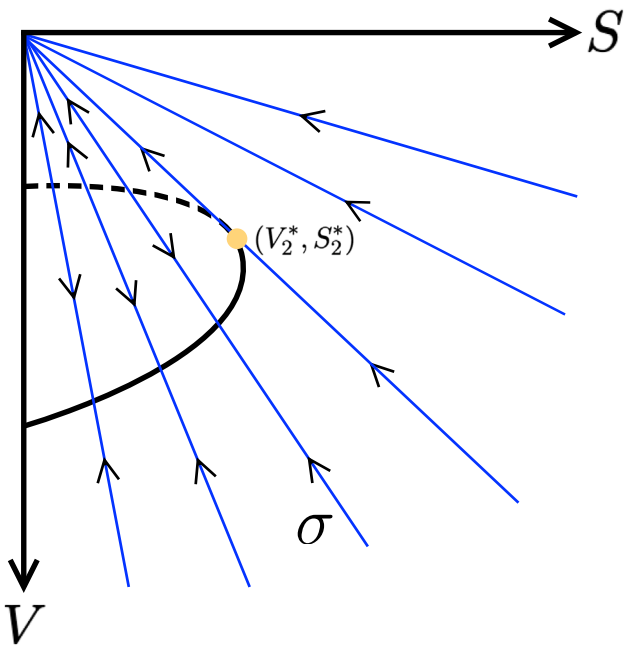

Fig. 2. Projection of the solutions of Eqs. (1)–(4) onto the plane (V, S) for $\alpha(1-\omega) = \beta$. The arrows indicate the direction of the orbits in positive time.

points $\{Q_2^r, Q_2^a\}$[4] that, recall, are equilibrium points. Then σ is the orbit of system (1)–(4) connecting these two points (in infinite time) with a heteroclinic connection. Thus, one of the equilibrium points, say Q_2^r, must have a 1-dimensional unstable invariant curve that coincides with σ and the other one, Q_2^a, must have a 1-dimensional stable invariant curve that matches σ. Notice that, in particular, these point-to-point in Γ heteroclinic connections fall within the more general homoclinic invariant manifold of the curve Γ to itself.

Consequently, the curve Γ splits into a stable branch Γ_a [red solid curve in Fig. 3(b)] and an unstable branch Γ_r [red dashed curve in Fig. 3(b)], both joined by orbits (in gray) whose projection on the (V, S, D)-space are straight lines. The point $Q_2^* \in \Gamma$ separating these two branches [dark-green dot in Fig. 3(b)] belongs to the straight line σ in $S/V = c^*$, contained in Π_{DV}, which is tangent to Γ. The projection of such orbits on the plane (V, S) is displayed in Fig. 2. The local stability of the equilibrium points $Q_2 \in \Gamma$ is determined by the eigenvalues of the differential matrix of system (1)–(4) when evaluated at Q_2. In its general form, it is given by:

$$DF(Q_2) = \begin{pmatrix} -\beta V_2 p_2 & -\beta V_2 p_2 & -\beta V_2 p_2 & \varepsilon V_2/p_2 \\ -\beta S_2 p_2 & -\beta S_2 p_2 & -\beta S_2 p_2 & \varepsilon S_2/p_2 \\ A_1 & A_2 & A_3 & A_4 \\ \kappa(1-p_2) & 0 & 0 & -\kappa V_2 - \varepsilon_p \end{pmatrix}, \tag{18}$$

where

$$A_1 = \frac{\varepsilon(\alpha-\beta)}{\beta} - p_2(V_2(\alpha-\beta) + \gamma D_2),$$
$$A_2 = -p_2(V_2(\alpha-\beta) + \gamma D_2),$$
$$A_3 = \frac{\varepsilon\gamma}{\beta} - p_2(V_2(\alpha-\beta) + \gamma D_2) - \varepsilon,$$
$$A_4 = \frac{\varepsilon}{p_2\beta}(V_2(\alpha-\beta) + \gamma D_2).$$

Recall that the values of V_2, D_2, p_2 of $Q_2 \in \Gamma$ are given, respectively, by the roots of (14) and expressions in (13), for $S_2 \in (0,1)$. For any Q_2, the corresponding Jacobian matrix (18) has a zero eigenvalue (a neutral direction) which corresponds to the tangent direction to Γ contained in Π_{DV}. The stable [Γ_a, continuous red curve in Fig. 3(b)] and unstable [Γ_r, dashed red curve in Fig. 3(b)] branches constituting Γ join at the point $Q_2^* \in \{S/V = c^*\} \cap \Pi_{DV}$. The value of c^* can be analytically computed and is given by

$$c^* = \frac{\kappa\beta}{4\varepsilon\varepsilon_p}\left(1 - \frac{\varepsilon}{\beta}\right)^2 - 1 - \frac{\alpha\omega}{\beta-\gamma}, \tag{19}$$

and its corresponding V_2 and S_2 coordinates are:

$$V_2^* = \frac{2\varepsilon\varepsilon_p}{\kappa(\beta-\varepsilon)}, \qquad S_2^* = \frac{2\varepsilon\varepsilon_p}{\kappa(\beta-\varepsilon)}\left(\frac{\kappa\beta}{4\varepsilon\varepsilon_p}\left(1 - \frac{\varepsilon}{\beta}\right)^2 - 1 - \frac{\alpha\omega}{\beta-\gamma}\right). \tag{20}$$

In addition to this common zero eigenvalue (associated to Γ), the differential matrix $DF(Q_2)$ for $Q_2 \in \Gamma_a$ has three real negative eigenvalues [two in (V, S, D)], and so it is of attracting type. On the other hand, any point $Q_2 \in \Gamma_r$ has three real eigenvalues, two negative and one positive. So, it is of saddle type, with a 1-dimensional unstable invariant curve. Regarding the junction point Q_2^*, its differential matrix has an extra zero eigenvalue. In some sense this fact can be seen as a kind of transcritical bifurcation *inside* Γ: one of the real eigenvalues of the equilibrium points filling Γ_r changes its sign when it crosses Q_2^*, moving along Γ in the direction of Γ_a. The location of the point Q_2^* in Γ depends on the rest of the parameters of the system. This is shown in Fig. 4(a), which displays the coordinates of equilibrium points Q_2 in Γ as a function of S^*. All these eigenvalues have been numerically computed during the simulations.

This particular type of invariant curves (like Γ), formed by equilibrium points, has been usually referred in the literature as *quasi-neutral* curves [22–30].

3.4. Global bifurcation associated with the breakdown of Γ

As seen in Section 3.2, three different kinds of equilibrium points may exist depending on the parameter values: the origin Q_0 as a coextinction state, the satellite-free state Q_1, and the coexistence of the three viral populations and the RdRp, Q_2. The latter, which exists only under specific conditions, leads to the following definition.

Definition 1. The *critical replication rate of HV*, denoted by α^*, is the value of α satisfying

$$\alpha^*(1-\omega) = \beta. \tag{21}$$

Thus, if α is taken as a bifurcation parameter, we denote by

$$\mu = \alpha - \alpha^* \tag{22}$$

the distance to this critical value. It satisfies $\mu > 0$ for $\alpha > \alpha^*$ and $\mu < 0$ for $\alpha < \alpha^*$.

The critical rate α^* corresponds to the precise value α (provided $\beta > \gamma$ also holds) at which the curve Γ of coexistence equilibrium points Q_2 exists, already analyzed in Section 3.3. From a biological viewpoint, this case implies the equality between the effective replication rate of HV and the satRNA's replication rate.

The aim of this section is to study this global bifurcation - that we have named *quasi-neutral nullcline confluence* (QNC) bifurcation - that system (1)–(4) undergoes at $\mu = 0$ (for $\beta > \gamma$). As far as we know, this type of bifurcation has not been previously described. This change in the dynamics is linked to an abrupt transition from a monostability to a bistability global scenario. The relevance of this case is that such bifurcation shows up through the exceptional appearance and breakdown of the quasi-neutral curve of coexistence equilibria Γ. Even more, the locally attractive property of this curve for $\mu = 0$ will make, for values of $\mu \sim 0$, that nearby orbits (a remarkable domain in the (V, S, D)-space) will be confined in a kind of bottleneck around the location where Γ was in the phase space for $\mu = 0$. This confinement will result in a slowing down of the dynamics of these orbits and in the emergence of extremely long transients.

[4] Superscripts r and a stand for, respectively, repeller and attractor.

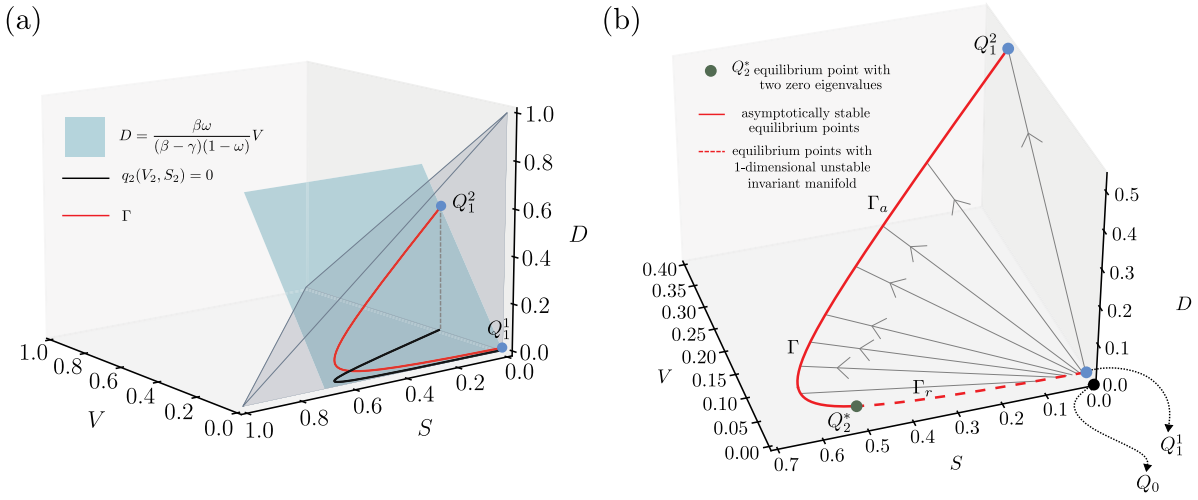

Fig. 3. (a) Projection of the quasi-neutral curve Γ (red) onto the space (V, S, D). Γ is contained in the invariant plane Π_{DV} (blue surface) and embedded into the projection of $\mathcal{U}$ onto (V, S, D) (gray tetrahedron). (b) Schematic projection in the space (V, S, D) of the heteroclinic connections among Q_2-points in Γ. Notice that, in particular, these connections belong to the homoclinic invariant manifold of the curve Γ itself. The heteroclinic connections (straight lines) go in infinite time from the unstable equilibrium points in Γ_r (dashed red curve) to the locally attracting equilibrium points of the piece of curve Γ_a (in solid red color). The dark-green point in Γ separates both branches, being tangent to the plane $S/V = c^*$ and having two zero eigenvalues in its Jacobian matrix. The equilibrium points Q_1^1 and Q_1^2 (in light blue color) represent the intersection of Γ with the invariant plane $\{S = 0\}$. The values of the parameters used to compute numerically Γ in (a) and (b) are given by $\alpha = 0.875$, $\beta = 0.7$, $\omega = 0.2$, $\gamma = 0.6$, $\kappa = 0.3$, $\varepsilon = 0.1$ and $\varepsilon_p = 0.01$. (For interpretation of the references to color in this figure legend, the reader is referred to the web version of this article.)

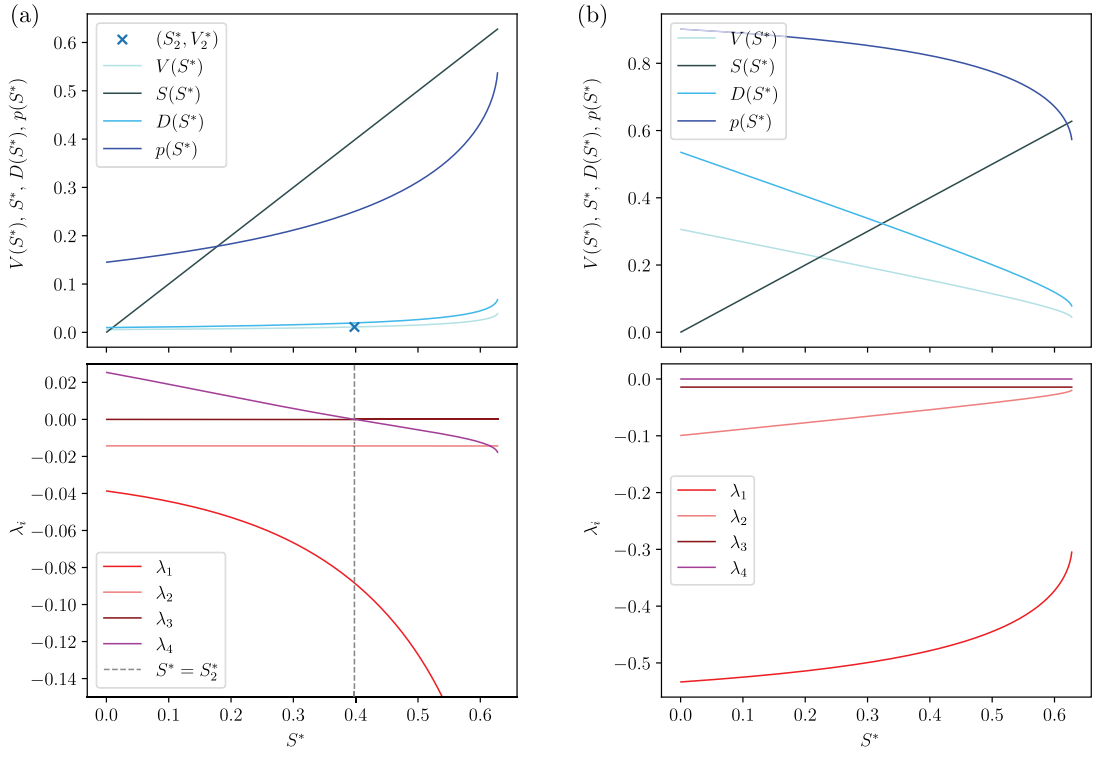

Fig. 4. Coordinates of equilibrium points Q_2 filling Γ (upper panels) and the corresponding eigenvalues of their differential matrix (lower panels). The parameter values used satisfy conditions in (12) and are given by $\alpha = 0.875$, $\beta = 0.7$, $\omega = 0.2$, $\gamma = 0.6$, $\kappa = 0.3$, $\varepsilon = 0.1$ and $\varepsilon_p = 0.01$. Panels (a) and (b) are related, respectively, to the two possible expressions for V_2 given by (16). The point (S_2^*, V_2^*), marked with a cross, is given by expression (20) and corresponds to the (V, S)-coordinates of Q_2^*.

In detail, this bifurcation takes place when the nullclines given by the parallel hypersurfaces

$$H_1 : \ p\Omega(x) = \frac{\varepsilon}{\alpha(1-\omega)} \qquad \text{and} \qquad H_2 : \ p\Omega(x) = \frac{\varepsilon}{\beta},$$

coincide at $\mu = 0$ and give rise to the curve of equilibria Γ, which only exists in such a case. To determine the role of the QNC bifurcation in organizing the dynamics, we study them in a neighborhood $\mu = 0$. First, we focus on the possible ω-limit sets of the orbits in $\mathring{\mathcal{U}}$ for $\mu < 0$ and $\mu > 0$. Numerical evidence discards chaotic behavior of the system, and since Proposition 1 states the non-existence of periodic orbits, we assume hereafter that the ω-limit scenarios must be either an equilibrium point of satellite extinction $Q_1 \in \{S = 0\}$ or the origin Q_0 itself (total extinction). The numerical integrations to obtain

the solutions of the ODEs have been performed using a Runge–Kutta-Fehlberg-Simó method[5] of order 7–8 with automatic step size control and local relative tolerance 10^{-15}.

The two leading parameters conducting this study are the replication rate of the HV (α) and that of the satRNA (β) since they establish the progeny production pace and thereby determine the persistence of the infection. On the other hand, DIPs are a byproduct of the HV dynamics, and the RdRp (p) plays a role subjugated to the HV. Therefore, for this reason, whenever numerical simulations are performed, α and β will vary while the rest of the parameters are assumed to take the following values:

$$\kappa = 0.3, \quad \omega = 0.2, \quad \gamma = 0.6, \quad \varepsilon = 0.1, \quad \varepsilon_p = 0.01. \tag{23}$$

These values are chosen to illustrate various infection dynamics by time series and provide visual information on transients. That is, we use small RNA degradation rates for the V, S, and D genomes compared to the (higher) amplification rate of these genomes to ensure initial progress of the infection. In addition, we also assume a low rate of the RdRp degradation to ensure replication progress.

The term $p\,\Omega(x)$ indeed plays a central role in the dynamics, acting as an effective logistic-like function, encompassing available resources for both RNA species and the amount of the RdRp enzyme. Below, we state its value on the feasible equilibrium points.

Lemma 5. *The function $p\,\Omega(x)$ vanishes at the origin, i.e., $p\,\Omega(x)\big|_{Q_0} = 0$.*

Lemma 6. *For any satRNA-extinction equilibrium point Q_1, we have* $p\,\Omega(x)\big|_{Q_1} = \dfrac{\varepsilon}{\alpha(1-\omega)}$.

3.4.1. Dynamics for $\mu < 0$

Let us consider the situation previous to the QNC-bifurcation (considering increasing values of $\alpha > 0$), that is, for $\mu = \alpha - \alpha^* < 0$ small. Lemmas 5 and 6 provide insights on the possible ω-limit sets in this regime by studying the term $p\,\Omega(x)$. Recall that the system does not admit periodic solutions, and numerics do not show other situations like chaotic or quasiperiodic behavior. Precisely, we have:

Proposition 6. *Let $\varphi(t, y_0)$ be the solution of (1)–(4) with initial condition $\varphi(0, y_0) = y_0 \in \mathring{\mathcal{U}}$. Then, its ω-limit $\omega(\varphi)$ satisfies that*

$$\omega(\varphi) = \lim_{t\to+\infty} \varphi(t, y_0) = Q_0, \tag{24}$$

where $Q_0 = (0, 0, 0, 0)$.

Remark 2. This statement also holds for orbits with initial conditions on $\{V + S + D = 1\}$, $D \in \{0, 1\}$ and $p \in \{0, 1\}$.

The studied system exhibits then monostability provided $y_0 \notin \{S = 0\}$. From $\mu < 0$ it easily follows that

$$\frac{\varepsilon}{\beta} < \frac{\varepsilon}{\alpha(1-\omega)}.$$

Taking this fact into account, Proposition 6, and Lemma 5, we get that, for any orbit φ with initial condition $y_0 \in \mathring{\mathcal{U}}$, there exists a minimal time value $0 \le \tau_1 < +\infty$ such that

$$p\,\Omega(x)\Big|_{x=\varphi(t,y_0)} < \frac{\varepsilon}{\beta}, \qquad \forall t > \tau_1, \tag{25}$$

This τ_1 depends on the initial condition y_0. Define now, for $\varphi(t, y_0) = (x(t), p(t))$, the following set:

$$D_{\varphi,y_0} = \left\{ 0 \le t < \tau_1 \;\middle|\; p(t)\Omega(x(t)) = \frac{\varepsilon}{\beta} \quad \text{or} \quad p(t)\Omega(x(t)) = \frac{\varepsilon}{\alpha(1-\omega)} \right\}. \tag{26}$$

This set contains all the time instants at which the orbit $\varphi(t, y_0)$ intersects either the nullcline H_1 or H_2. In the case that D_{φ,y_0} is non-empty, we define $\tau_0 > 0$ as

$$\tau_0 = \sup(D_{\varphi,y_0}). \tag{27}$$

Essentially, $[\tau_0, \tau_1]$ is the last time interval in which $\varphi(t, y_0)$ is contained among both nullclines. These definitions provide insights on the behavior of $S(t)$ before reaching its ω-limit. We cannot provide any analytic expression (in the case it would exist) for the dependence of (τ_0, τ_1) in terms of the initial conditions of the orbit. Their computation is always achieved by numerically integrating the orbits and controlling the nullclines crossing. In any case, the following result holds:

Lemma 7. *Let us assume that for an orbit $\varphi(t, y_0) = (V(t), S(t), D(t), p(t))$ with $y_0 \in \mathring{\mathcal{U}}$, the values τ_0 and $\tau_1 > 0$ exist. Then $S(t)$ has a local maximum at $t = \tau_1$ and it is monotonously decreasing for all $t > \tau_1$.*

Notice that, from the equation satisfied by $\dot{S}$, $S(t)$ grows in all the time intervals in which $p\,\Omega(x)$ falls between $\frac{\varepsilon}{\beta}$ and $\frac{\varepsilon}{\alpha(1-\omega)}$, and not only in the interval (τ_0, τ_1). Moreover, for those orbits $\varphi(t, y_0)$ with initial condition $y_0 = (V_0, S_0, D_0, p_0)$ for which we can define τ_0 (*i.e.*, those with non-empty D_{φ,y_0}), a lower bound for the length of the interval (τ_0, τ_1) can be proved.

Proposition 7 ($p\,\Omega(x)$ *Scaling-Law for $\mu < 0$*). *Let $\mu < 0$ and φ defined as above with initial conditions satisfying $S(0), V(0) \neq 0$ and D_{φ,y_0} non-empty. Then, there exists a constant $\tilde{K}$, which depends on the parameters of the system but independent of μ, such that*

$$\tau_1 - \tau_0 > \frac{\tilde{K}\alpha}{\varepsilon}\frac{1}{|\mu|}, \tag{28}$$

where $\tilde{K}$ is given by

$$\tilde{K} := \max\left\{ \log\left(\frac{V_0}{V_1}\right), \log\left(\frac{S_1}{S_0}\right) \right\}, \tag{29}$$

with $V_0 = V(\tau_0)$, $V_1 = V(\tau_1)$, $S_0 = S(\tau_0)$ and $S_1 = S(\tau_1)$.

Remark 3. In other words, $p\,\Omega(x)$ remains inside $\left(\frac{\varepsilon}{\beta}, \frac{\varepsilon}{\alpha(1-\omega)}\right)$ for all $t \in (\tau_0, \tau_1)$, where

$$\tau_1 - \tau_0 \sim O\left(\frac{1}{|\mu|}\right), \tag{30}$$

provided that $\tilde{K}$ is, at least, $O(\varepsilon)$.

Since the coordinate hypersurfaces $\{S = 0\}$ and $\{V = 0\}$ are invariant by the flow, the solution $\varphi(t, y_0)$ can never reach them whenever its initial condition falls in $\mathring{\mathcal{U}}$. The scaling law for $p\Omega(x)$ stated in Proposition 7 can be numerically observed for all four variables, $V(t), S(t), D(t)$, and $p(t)$. Indeed, for small values of μ, long transients appear when orbits φ evolve close to where Γ will be located in the case $\mu = 0$, when the QNC bifurcation occurs. They behave as if retained by a kind of bottleneck or ghost curve during long time intervals. The distance of φ to this ghost curve is represented by the red curve in Fig. 6(a) and their dynamics are illustrated in Fig. 6. Long transients in these temporal series must be compared with those in Fig. 5(a), where the time spent to reach a neighborhood of the equilibrium Q_0 is five orders of magnitude smaller since the system is far from the bifurcartion.

Fig. 6(a) also shows different transients experiencing these delays. Three different orbits with different initial conditions (green colors) are represented, also displayed in the (V, S) space. Their dynamics here are characterized by a fast approach towards the bottleneck followed by a very slow passage throughout it. Numerical results have revealed that for values of $|\mu| \to 0$, the time needed to reach a fixed neighborhood of Q_0 behaves like $t \sim |\mu|^{-1}$. This scaling law is definitely determined by the proximity between the two nullclines H_1 and H_2 when $\mu < 0$ is small. Additionally, some examples of the monostable scenario provided in Proposition 6 are shown in Figs. 1(b) and 6(b).

[5] with an improvement by Prof. Lluís Alsedà.

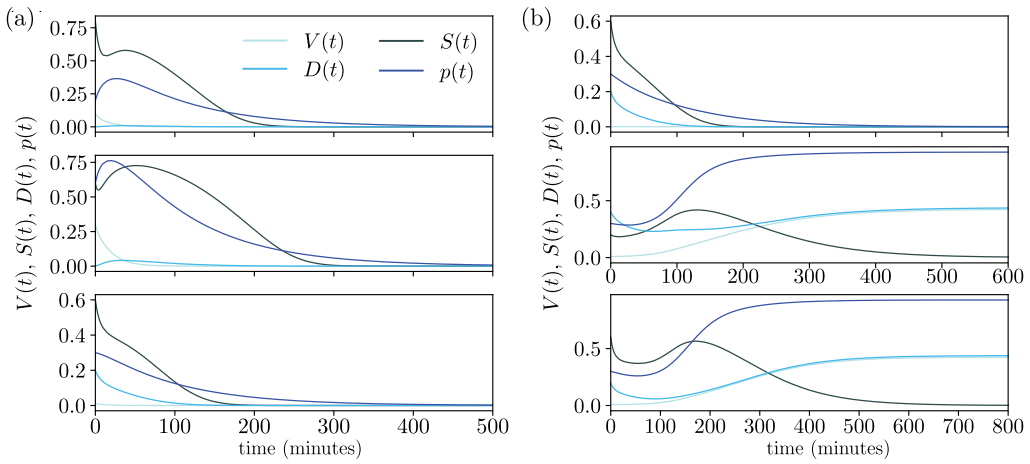

Fig. 5. Numerically computed time series for (a) $\alpha = 0.375 < \alpha^*$ ($\mu < 0$) and (b) $\alpha = 0.99 > \alpha^*$ ($\mu > 0$), both with $\beta = 0.7$ and the rest of the parameters as given in (23), thus with $\alpha^* = 0.875$. Both cases correspond to a region of the space of parameters ($|\mu| > 0.1$) far from the global bifurcation value at $\mu = 0$. Each panel has been obtained with different initial conditions. Panels in (a) correspond to monostability; panels in (b) display the bistability scenario, where both the origin and the satRNA-extinction equilibrium point Q_1 are locally asymptotically stable. Notice that, far from the bifurcation, transient times are short (cf. Figs. 6–8 with transients close to the bifurcation threshold).

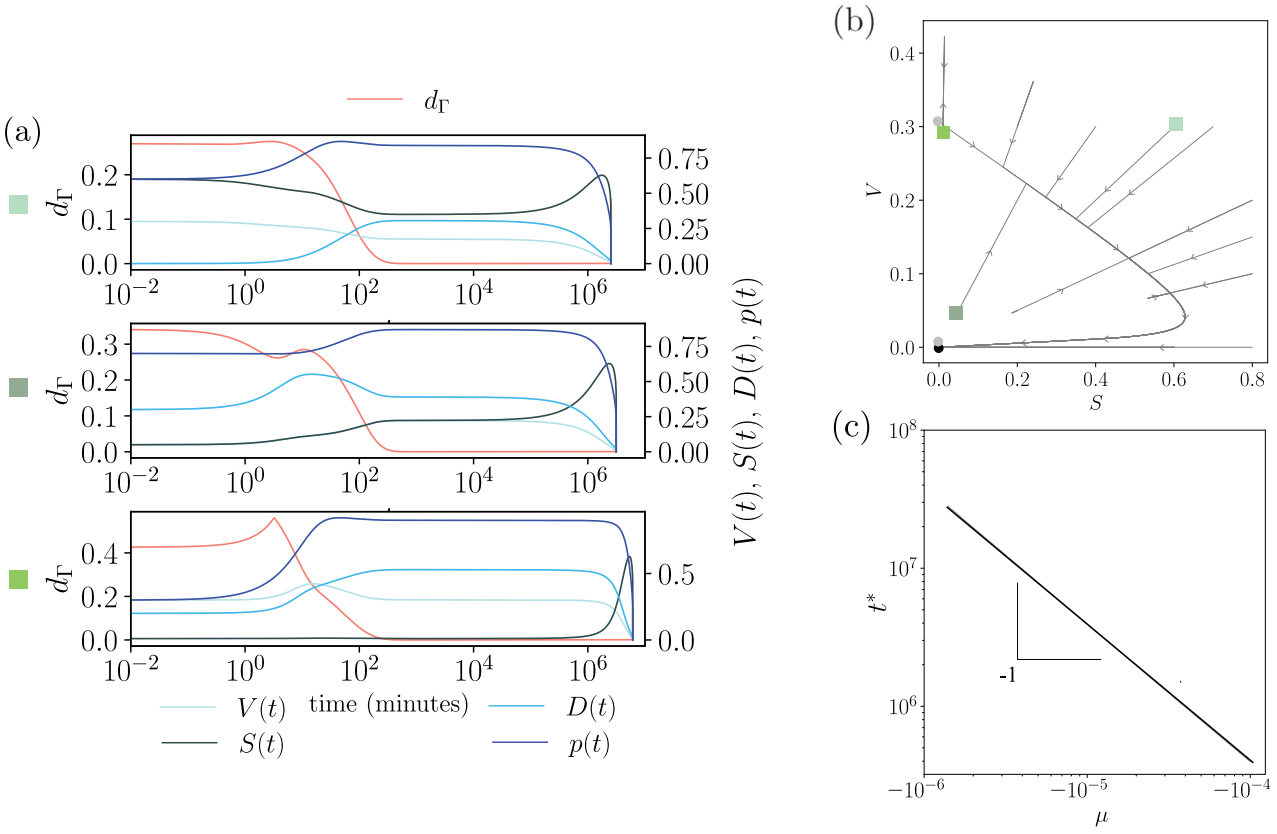

Fig. 6. (a) Long transients around the remnant of the curve Γ close to the QNC bifurcation with $\mu = -10^{-5}$. Here the origin is a global attractor, and the system becomes extinct for any initial condition with $S_0 \neq 0$. The red line shows how the distance from the orbit to the coordinates of Γ changes over time. Each panel displays the time series for a specific initial condition, identified by a green-colored square in (b). (b) Phase portrait with several orbits shown projected into the plane (S, V). Here, the black and gray dots are local attractors and saddle points, respectively. (c) Times needed to reach a neighborhood of the origin numerically computed as a function of the distance to the bifurcation value μ, which follows the scaling law $t^* \sim |\mu|^{-1}$. Here, we use $(V_0, S_0, D_0, p_0) = (0.5, 0.2, 0, 0)$. Simulations in (a-c) have been performed using the values of the parameters in (23), $\beta = 0.7$ and $\alpha = 0.87499$. (For interpretation of the references to color in this figure legend, the reader is referred to the web version of this article.)

Fig. 7(a) displays the time series evolution for a given orbit φ and its corresponding value $p\,\Omega(x)$.

This time scaling provides analytical and numerical results that could be related to biological chronic infections in terms of (long) transient states. Long transients involve non-zero populations for large periods of time in such a way that coexistence is allowed, although not being the final stable state. However, we must notice that these dynamics may be found close to bifurcation thresholds. That is, with parameter values far from the bifurcation value $\mu = 0$ the transients appear to be fast. In the long term, since the intrinsic replication rate of the satRNA, β, is larger than the one of the HV, α, the latter is unable to survive due to possibly a satRNA population consuming resources at

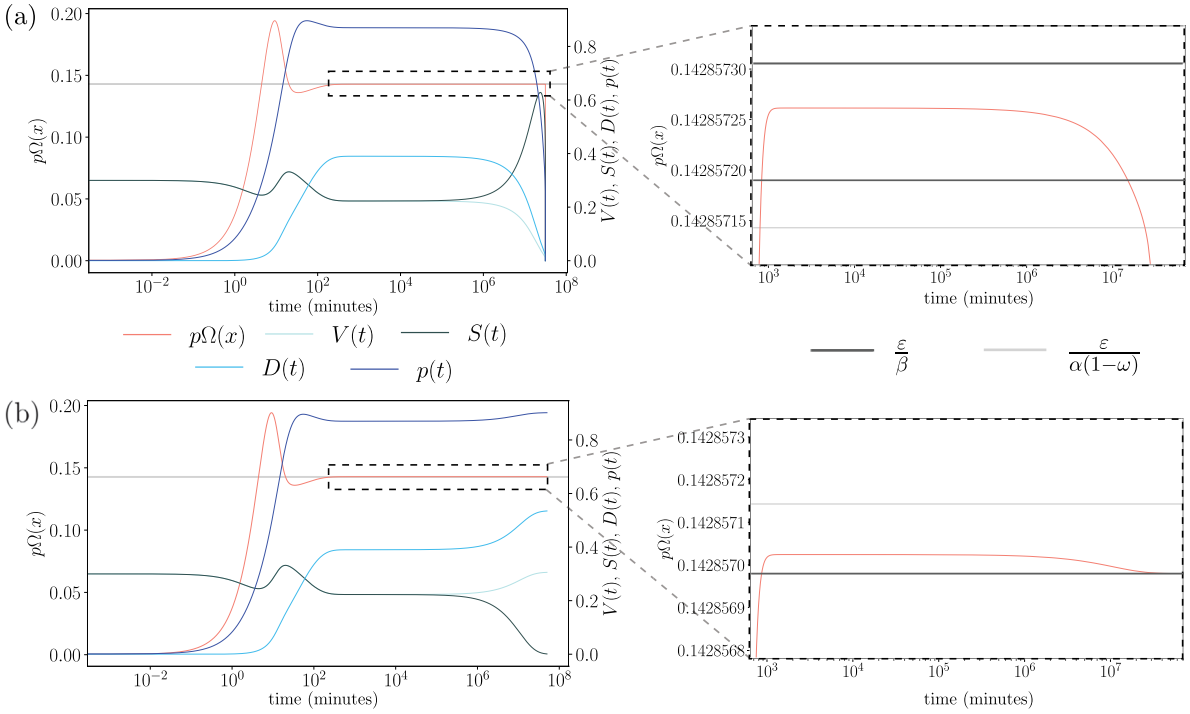

Fig. 7. Time evolution of the four variables for two different values of α satisfying $\mu \approx 0$ along with the time evolution of $p\,\Omega(x)$ (red curve). The values of the parameters used to perform numerical simulations in (a) and (b) are given by (23) for κ, ω, γ, ε and ϵ_p; by $\beta = 0.7$ and by $\alpha = 0.874999$ in (a) and $\alpha = 0.875001$ in (b). Panel (a) displays the dynamics for $\mu < 0$ while panel (b) for $\mu > 0$. Thus, both regimes are within a neighborhood of the region at which the system undergoes a global bifurcation. Long transients are observed for both the state variables and the function $p\,\Omega(x)$. Initial conditions used in time series in (a) and (b) are given by $(V_0, S_0, D_0, p_0) = (0.3, 0.3, 0, 0)$. (For interpretation of the references to color in this figure legend, the reader is referred to the web version of this article.)

a higher pace and so driving the infection to the complete extinction. The second panel in Fig. 10(b) reflects this behavior in the basin of attraction of the origin.

The outcome differs drastically for initial conditions satisfying $S_0 = 0$. The invariance of this hyperplane allows equilibria state combining non-all-vanishing HV, DIPs and RdRp. In this regime, when the condition for the existence of equilibrium Q_1 [see Eq. (10)] is fulfilled, there exist two non-trivial equilibrium points of this type, say Q_1^1 and Q_1^2. Their location in $\{S = 0\}$ depends on the value of the parameter α and is coincident for a particular value α_*, denoted by a gray dot in Fig. 9. For $\alpha < \alpha^*$ (i.e. $\mu < 0$) both points are of saddle type: one with three attracting directions and one repelling, which is the attractor for orbits with initial conditions in $S = 0$; and the other, the other way round. The evolution of Q_1^1 and Q_1^2 for increasing values of $\alpha < \alpha^*$ is shown in Fig. 9. The direction of the blue arrows corresponds to growth in the value of α. According to the second panel in Fig. 10(b), only large values of α satisfying $\mu < 0$ allow coexistence of V, D, and p inside the invariant set $\{S = 0\}$.

3.4.2. Dynamics for $\mu > 0$

In this case, the effective replication rate of V, given by $\alpha(1-\omega)$, satisfies $\alpha(1-\omega) > \beta$ and so HV replicates faster than the satRNAs. Consequently, one of the two equilibria of type Q_1 becomes locally stable, as well as the origin. The system exhibits bistability: total extinction or a satRNA-extinction steady state [see the phase portraits of Figs. 1(d) and 8(b) and in the time series of Fig. 8(a)].

For those orbits whose ω-limit is an equilibrium point of type Q_1, the following result holds:

Proposition 8 (Q_1 *as* ω*-Limit*). *Consider a solution* $\varphi(t, y_0)$ *of system (1)–(4), with initial conditions* $y_0 = (V_0, S_0, D_0, p_0)$ *and* $V_0 \neq 0$*, whose* ω*-limit set is an equilibrium point of type* Q_1*. Then, for any arbitrarily small* $\xi > 0$ *there exists a time* $T = T(\xi)$ *such that the associated function* $p(t)\,\Omega(x(t))$ *is confined in*

$$\left(\frac{\varepsilon}{\alpha(1-\omega)} - \xi, \frac{\varepsilon}{\alpha(1-\omega)} + \xi\right) \tag{31}$$

for $t > T$.

So, in that case, the orbit $\varphi(t, y_0) = (x(t), p(t))$ gets trapped for infinite time in a neighborhood of the nullcline H_1. In other words, it gets confined inside a bottleneck around the location where the quasi-neutral curve Γ emerged for $\mu = 0$.

Further discussion can be done about this bistability scenario using a numerical example. Consider the values of the parameters in (23) and $\mu = 10^{-5}$. As already known, three equilibrium points exist belonging to $\{S = 0\}$: the origin Q_0, which is an attracting node, Q_1^1 a saddle, and Q_1^2 also an attracting node. More precisely, the points Q_1^1 and Q_1^2 come from a couple of points Q_1 in the case $\mu = 0$. This couple is depicted as light blue dots in Fig. 9 and, as end-points of the curve Γ, they have a local 1-dimensional neutral direction, transversal to $\{S = 0\}$. Once the quasi-neutral curve Γ is broken, *i.e.* μ becomes positive and small, the stability of these points changes: Q_1^2 becomes an attracting node while Q_1^1 a saddle point (see Fig. 9) with a 1-dimensional unstable invariant manifold $W^u(Q_1^1)$ and a 3-dimensional stable invariant manifold $W^s(Q_1^1)$. The latter is a hypersurface embedded in the 4-dimensional space (V, S, D, p) and, therefore, it splits the whole space into two disjoint subspaces, acting as a *separatrix* for the basins of attraction of both points Q_0 and Q_1^2. This splitting is also preserved by projection on the (V, S, D)-space. While dynamics of orbits $\varphi(t, y_0)$ have been observed numerically to be fast for those orbits with ω-limit the origin, Q_0, [third panel in Fig. 8(a)], for those orbits with initial conditions y_0 in the basin of attraction of Q_1^2, their dynamics appear to be slow for small $\mu > 0$ and long transients are observed, as displayed in the first and second panels of Fig. 8(a).

In this scenario, a hypothetical infection with an initial low viral load of the HV and a large proportion of satRNAs may be driven to complete extinction, establishing an initial population threshold of the

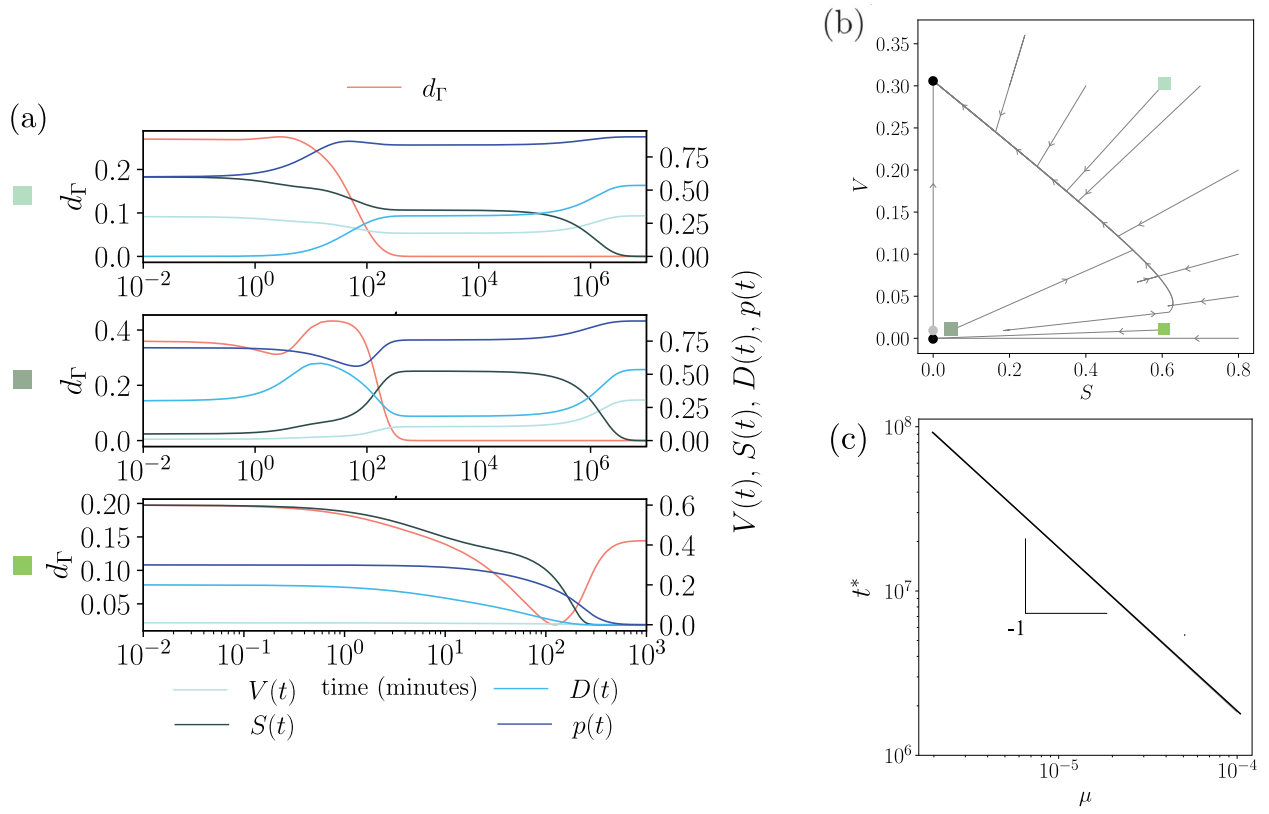

Fig. 8. Analogous to Fig. 6 with $\mu = 10^{-5}$, where the system is bistable. (a) The two upper plots show the satRNA extinction and the distance (red line) of the orbit to Γ coordinates (recall Γ only exists for $\mu = 0$), for two initial conditions identified with colored squares in the phase portrait in panel (b). The lower plot in (a) shows the full extinction since the orbit starts inside the basin of attraction of the origin. (c) The same scaling law for the transients close to the bifurcation threshold is identified here numerically. Simulations in (a-c) have been performed using the values of the parameters in (23), $\beta = 0.7$ and $\alpha = 0.87501$. (For interpretation of the references to color in this figure legend, the reader is referred to the web version of this article.)

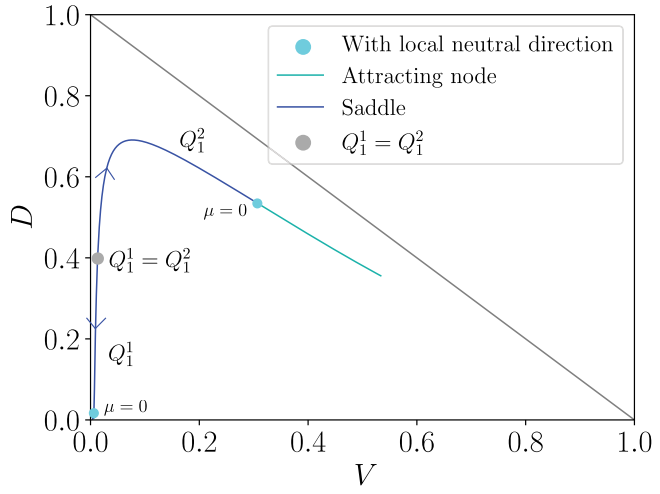

Fig. 9. Evolution of the equilibrium points of type Q_1 and their local stability in the phase plane (V, D) at increasing α (and so of $\alpha(1-\omega)$) for parameter values in (23) and $\beta = 0.7$. The blue arrows indicate the direction of increasing values of α. Light blue dots correspond to the case $\mu = 0$, when the system undergoes the global bifurcation. The gray line denotes the limit of the meaningful domain in the (V, D) space. (For interpretation of the references to color in this figure legend, the reader is referred to the web version of this article.)

HV in order to achieve a persistent infection. Orbits with the origin as ω-limit [see the bottom panel in Fig. 8(a) and the fourth panel in Fig. 10(b)] are faster in reaching a vicinity of the equilibrium state since they are not affected by the *ghost* of the quasi-neutral curve Γ. Orbits exhibiting long transients seem to satisfy also a scaling power law for their time length of type $t \sim O(|\mu|^{-1})$. This law has been found numerically for orbits within the basin of attraction of Q_1^2, see Fig. 8(c). Furthermore, the result in Proposition 8 has been checked numerically in this case. See Fig. 7(b), where the term $p\,\Omega(x)$ gets trapped between the nullclines H_1 and H_2 despite the populations keeping changing over time.

Finally, a numerical study of the basins of attraction of the different equilibrium points has been carried out in terms of γ [see Fig. 10(a)]. A replication rate of the DIPs (γ) larger than that of the satRNA (β) leads to the total extinction of populations due to DIPs consuming resources at a higher rate. Since they are dependent on the RdRp produced by the HV, the exhaustion of resources causes the HV extinction and, consequently, it halts the production of RdRp, driving the remaining RNA molecular species to extinction.

4. Discussion

Understanding the interaction among different viral agents replicating within the same host cell is crucial to determine the fate of viral infections. A very well-studied case is the replication of a wild-type (wt) virus (also called helper virus, HV) together with its defective viral genomes (DVGs) [6]. DVGs are deletion mutants lacking essential viral genes and are spontaneously synthesized during the regular replication of the wt virus. Some of them are usually referred to as defective interfering particles (DIPs) when they interfere in the replication and virion assembly of the HV. DIPs can reduce the symptoms caused by the HV [14,15,46], modulate virulence [47] or even worsen such symptoms [18,48]. Considerable research has been performed on wt virus-DIPs in the last decades, including experimental [23,49–54],

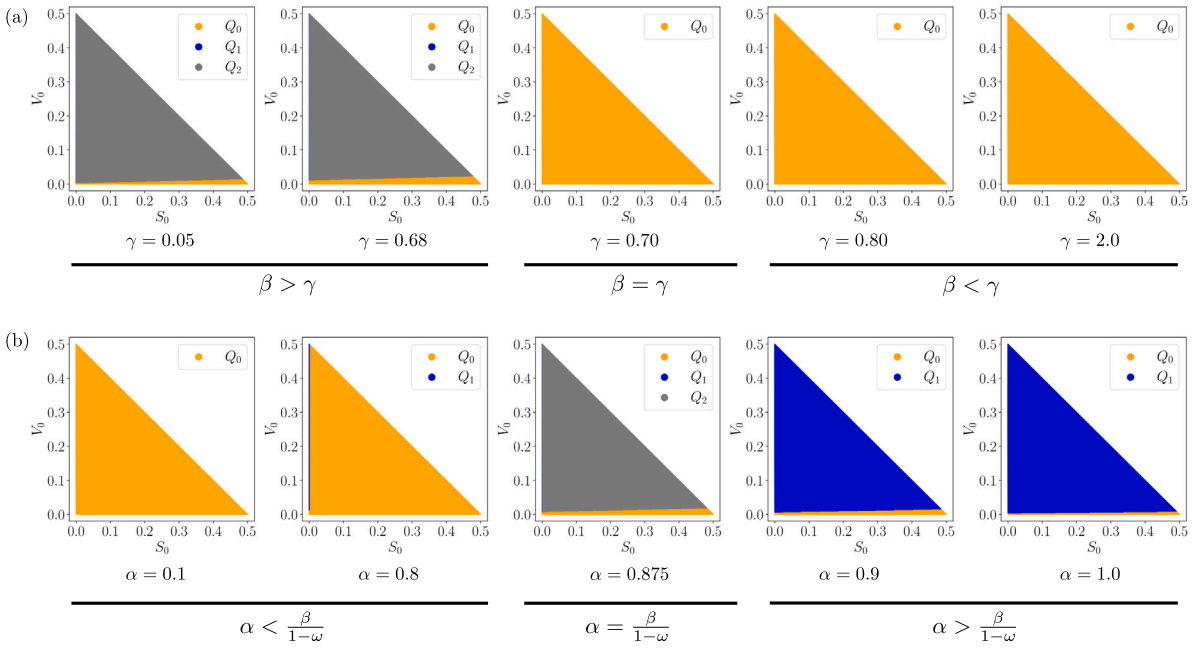

Fig. 10. Basins of attraction for different values of the parameters in the plane of initial conditions (S_0, V_0) (assuming HV-satRNA coinfections). The achieved ω-limits for the initial conditions are shown with different colors: full extinction (orange); HV-DI-RdRp coexistence and satRNA extinction (blue); and full coexistence (gray). (a) Basins of attraction tuning γ with $\alpha = 0.875$, $\omega = 0.2$, $\varepsilon = 0.1$, $\varepsilon_p = 0.01$, $\kappa = 0.3$ and $\beta = 0.7$. The value of γ varies in three different regions: $\beta > \gamma$, for which the quasi-neutral curve exists; $\beta = \gamma$, critical value for which the quasi-neutral curve disappears; and $\beta < \gamma$, where only the origin and the satRNA extinction equilibrium exist. (b) Basins of attraction for different values of α with for $\omega = 0.2$, $\varepsilon = 0.1$, $\varepsilon_p = 0.01$, $\kappa = 0.3$, $\beta = 0.7$ and $\gamma = 0.6$. (For interpretation of the references to color in this figure legend, the reader is referred to the web version of this article.)

theoretical [55–59], and both approaches together [23,60,61].

Together with the coexistence of HV-DIPs inside the host cell, other subviral agents can coinfect or superinfect the host cells, introducing further complexity and nonlinearity to the dynamics. For instance, viral satellites or satellite RNAs (satRNAs) [8]. These subviral agents, which are not genetically related to the wt virus, also kidnap the products of the HV as DIPs do, *i.e.*, the RdRp and the structural proteins, competing for the cellular resources. Satellite infections, which are very common in plant viruses [8,14], can also occur in other organisms [11–13], including humans. For example, the hepatitis delta virus requires the presence of the hepatitis B virus for its spread. When coinfection of these two viruses occurs, the symptoms are much more severe, accelerating hepatic cirrhosis [18].

While the dynamics of HV-DIPs have been widely investigated over the last decades [49,54–56,58,59], the impact of virus satellites or satRNAs remains less explored. Few works have investigated the dynamics for these multiple-virus systems. For instance, Ref. [20] investigated a mass action model for an HV synthesizing DIPs and coinfecting with a satRNA. In this manuscript we investigate a similar system including the RdRp, which introduces further nonlinearity into the system. We have identified three possible regimes as a function of parameters, mostly depending on the balance between the effective replication rate of the HV $\alpha(1-\omega)$ and the satRNA's replication rate β. Here, α and ω are the HV replication rate and the rate of DIPs' production, respectively. For $\alpha(1-\omega) < \beta$, the satRNA replicates faster than HV, conducting the infection to its demise. For $\alpha(1-\omega) = \beta$, there exists a bistable scenario with full coexistence governed by a quasi-neutral curve of equilibria. Finally, for $\alpha(1-\omega) > \beta$, bistability is maintained, driving the system towards either the satRNA extinction or the full extinction depending on the initial conditions.

We show that the quasi-neutral curve, which is structurally unstable, is involved in a global bifurcation that we have named as *quasi-neutral nullcline confluence* (QNC) bifurcation. At the bifurcation value, two nullcline hypersurfaces coincide, giving rise to the curve of equilibria. In the neighborhood of this bifurcation, long transients have been observed, and their duration t is shown to follow scaling laws of the form $t \sim |\mu|^{-1}$, with $\mu = \alpha - \alpha^*$, α^* being the bifurcation value associated to the critical replication rate of the HV. Such a scaling law has been found numerically and derived analytically. This scaling exponent coincides with the one obtained in a host-parasite model with a quasi-neutral curve of equilibria [28]. Close to the bifurcation, the orbits are strongly conditioned by a ghost quasi-neutral curve, and an apparent state of persistent HV-DIPs-satRNAs infection arises.

As mentioned, Ref. [20] investigated the dynamics of a similar model without including the RdRp. This model revealed three different scenarios depending on parameter values: (*i*) full extinction; (*ii*) HV-DIPs coexistence with satRNA clearance; and (*iii*) HV-DIPs-satRNA coexistence. This system revealed a very narrow region of bistability allowing for scenarios (*ii*) and (*iii*) to coexist. Our results indicate that the explicit inclusion of the RdRp involves wider bistability scenarios, and full coexistence only governed by the quasi-neutral curve. Dynamics governed by quasi-neutral manifolds have been identified in Lotka–Volterra competition models [29], in strains' competition models of disease dynamics [62]. Within the field of theoretical virology, quasi-neutral lines have been investigated in simple models of asymmetric RNA replication [22]. More recently, planes of equilibria have been identified in epidemiological-like models for coronavirus infection in cell cultures [23].

Our results suggest that HV-DIPs-satRNA coexistence at early stages of replication could be governed by quasi-neutral manifolds or, more likely, by transients near the global bifurcation of the quasi-neutral curve. It is known that virus replication can be spatially structured within the cell. In this sense, viral replication factories could play a key role in promoting further coexistence of these viral agents [44]. Future research should focus on the impact of space on these quasi-neutral manifolds. To the extent of our knowledge, this topic has not yet been addressed. Also, the impact of noise on these neutral manifolds and on the identified scaling laws close to the bifurcation threshold may be worth to exploring within the context of coinfections and superinfections caused by viral satellites.

CRediT authorship contribution statement

Oriol Llopis-Almela: Writing – review & editing, Writing – original draft, Supervision, Software, Methodology, Investigation, Formal analysis, Data curation, Conceptualization. **J. Tomás Lázaro:** Writing – review & editing, Writing – original draft, Supervision, Software, Methodology, Investigation, Formal analysis, Data curation, Conceptualization. **Santiago F. Elena:** Writing – review & editing, Writing – original draft, Supervision, Methodology, Investigation, Data curation, Conceptualization. **Josep Sardanyés:** Writing – review & editing, Writing – original draft, Supervision, Project administration, Methodology, Investigation, Funding acquisition, Formal analysis, Data curation, Conceptualization.

Declaration of competing interest

The authors declare that they have no known competing financial interests or personal relationships that could have appeared to influence the work reported in this paper.

Acknowledgments

O.L has been supported by the predoctoral program AGAUR-FI ajuts (2023 FI-1 00354) Joan Oró, which is backed by the Secretariat of Universities and Research of the Department of Research and Universities of the Generalitat of Catalonia, as well as the European Social Plus Fund. J.T.L has been supported by the project PID2021-122954NB-I00 funded by MCIU/AEI/10.13039/501100011033/ and "ERDF a way of making Europe", and by the grant "Ayudas para la Recualificación del Sistema Universitario Español 2021-2023". J.T.L also thanks the Laboratorio Subterráneo de Canfranc, the I2SysBio and the Institut de Mathématiques de Jussieu-Paris Rive Gauche (Sorbonne Université) for their hospitality as hosting institutions of this grant. We also thank the MCIU/AEI/10.13039/ 501100011033/, through the María de Maeztu Program for Units of Excellence in R&D (CEX2020-001084-M) and CERCA Programme/Generalitat de Catalunya for institutional support. J.S has also been supported by the Ramón *y* Cajal grant RYC-2017-22243 funded by MCIU/AEI/10.13039/ 501100011033 and "ESF invests in your future". S.F.E was supported by grant PID2022-136912NB-I00 funded by MCIN/AEI/ 10.13039/501100011033 and by "ERDF a way of making Europe", and by Generalitat Valenciana, Spain grant CIPROM/2022/59. We would like to express our gratitude to three anonymous referees for their assistance in improving a previous version of the manuscript.

Appendix A. Equilibrium points and general dynamics

A.1. Proof of Lemma 1

Eq. (4) at the equilibrium reads as $\kappa V^*(1-p^*)-\varepsilon_p p^*=0$. Straightaway, it leads to expression

$$p^*=p^*(V^*)=1-\frac{\varepsilon_p}{\kappa V^*+\varepsilon_p}. \tag{32}$$

On the one hand, $\kappa V^*+\varepsilon_p \geq \varepsilon_p$, since $\kappa>0$, $\varepsilon_p>0$ and $V^*\geq 0$. Therefore, $0\leq p^*<1$ and $p^*(V^*)=0$ if and only if $V^*=0$.

A.2. Proof of Proposition 1

We prove the result by *reductio ad absurdum*. Let us assume there exists a solution of system (1)–(4) that is T-periodic with period $T>0$. This implies that all the variables of the solution must be T-periodic, *i.e.*, $V(t)$, $S(t)$, $D(t)$ and $p(t)$ are T-periodic. Focusing on $p(t)$, we can rewrite Eq. (4) as

$$\dot{p}(t)=-(\kappa V(t)+\varepsilon_p)p(t)+\kappa V(t), \tag{33}$$

which is a non-homogeneous 1st order linear differential equation that can be expressed as $\dot{p}(t)=a(t)p+b(t)$, where $a(t)=-(\kappa V(t)+\varepsilon_p)$ and $b(t)=\kappa V(t)$. General solution for this linear differential equation may be written as

$$p(t)=p_0\exp\left(\int_0^t a(s)ds\right)+\int_0^t b(r)\exp\left(\int_r^t a(s)ds\right)dr, \tag{34}$$

and, plugging the values of $a(t)$ and $b(t)$, we obtain:

$$p(t)=p_0\exp\left(-\varepsilon_p t-\kappa\int_0^t V(s)ds\right)+\kappa\exp(-\varepsilon_p t)\int_0^t V(r)\exp\left(\varepsilon_p r-\kappa\int_r^t V(s)ds\right)dr. \tag{35}$$

Defining

$$w(t)=p_0\exp\left(-\kappa\int_0^t V(s)ds\right)+\kappa\int_0^t V(r)\exp\left(\varepsilon_p r-\kappa\int_r^t V(s)ds\right)dr, \tag{36}$$

we can rewrite $p(t)$ as

$$p(t)=\exp\left(-\varepsilon_p t\right)w(t). \tag{37}$$

Since $p(t)$ is T-periodic, we have $p(0)=p(T)$ where $p(0)=p_0$ and $p(T)=\exp(-\varepsilon_p T)w(T)$. Then,

$$p_0=e^{-\varepsilon_p T}w(T)\Longleftrightarrow w(T)=p_0e^{\varepsilon_p T}.$$

Introducing the expression of $w(t)$ given by Eq. (36) in the last equality and rearranging terms, we obtain:

$$p_0\left(e^{\varepsilon_p T}-\exp\left(-\kappa\int_0^T V(s)ds\right)\right)=\kappa\int_0^T V(r)\exp\left(\varepsilon_p r-\kappa\int_r^T V(s)ds\right)dr. \tag{38}$$

We now consider two cases:

- Consider
$$e^{\varepsilon_p T}-\exp\left(-\kappa\int_0^T V(s)ds\right)\neq 0. \tag{39}$$
Then p_0 has the following expression:
$$p_0=\frac{\kappa}{e^{\varepsilon_p T}-\exp\left(-\kappa\int_0^T V(s)ds\right)}\int_0^T V(r)\exp\left(\varepsilon_p r-\kappa\int_r^T V(s)ds\right)dr. \tag{40}$$
This equation uniquely determines the initial value $p(0)=p_0$ that makes $p(t)$ to be T-periodic but there exist infinitely many possible values for p_0 on the periodic solution. Therefore, we have a contradiction.
- Consider now
$$e^{\varepsilon_p T}-\exp\left(-\kappa\int_0^T V(s)ds\right)=0. \tag{41}$$
Therefore,
$$\frac{1}{T}\int_0^T V(s)ds=-\frac{\varepsilon_p}{\kappa}, \tag{42}$$
which provides an expression for the mean value of function $V(t)$ in the interval $[0,T]$. However, by hypothesis we are considering initial conditions in $\mathcal{U}$ and, since this domain is positively invariant, $V(t)$ is a positive function within it. Therefore, its mean value cannot be negative.

Both cases lead to contradictions and, therefore, $p(t)$ cannot be periodic. Since there is a component in solution $(V(t),S(t),D(t),p(t))$ which is not T-periodic, solution cannot be T-periodic.

A.3. Proof of Lemma 2

For $V^* = 0$ we have $\dot{V} = 0$. Assuming it, equation $\dot{p} = 0$ only has $p^* = 0$ as a valid solution. Conditions $V^* = 0$ and $p^* = 0$ lead equation $\dot{D} = 0$ only to be satisfied for $D^* = 0$. Finally, $p^* = 0$ leads equation $\dot{S} = 0$ to be satisfied only when $S^* = 0$. Thus, for $V^* = 0$, the only equilibrium point possible is $Q^* = Q_0 = (0, 0, 0, 0)$.

A.4. Proof of Lemma 3

Equilibrium equation for V with the constraint $\alpha(1-\omega) = \gamma$ reads:

$$V^* (\gamma p \Omega(x) - \varepsilon) = 0, \tag{43}$$

which gives rise to two different cases: $V^* = 0$ or $p\,\Omega(x) = \varepsilon/\gamma$. Case $V^* = 0$ is already described in Lemma 2. Assume then $p\,\Omega(x) = \varepsilon/\gamma$. Equilibrium equation for D reads:

$$(\omega\alpha V^* + \gamma D^*)\frac{\varepsilon}{\gamma} - \varepsilon D^* = 0 \Longleftrightarrow \frac{\omega\alpha\varepsilon}{\gamma} V^* = 0. \tag{44}$$

Then, necessarily, one must have $V^* = 0$. Lemma 2 completes the proof.

A.5. Proof of Lemma 4

The differential matrix of system (1)–(4) evaluated at the origin is given by

$$DF(\mathbf{0}) = \begin{pmatrix} -\varepsilon & 0 & 0 & 0 \\ \kappa & -\varepsilon_p & 0 & 0 \\ 0 & 0 & -\varepsilon & 0 \\ 0 & 0 & 0 & -\varepsilon \end{pmatrix}, \tag{45}$$

with eigenvalues $\lambda_1 = -\varepsilon_p$ and $\lambda_2 = \lambda_3 = \lambda_4 = -\varepsilon$. Since we are assuming $\varepsilon_p, \varepsilon > 0$, all eigenvalues are real and negative and, therefore, the origin is locally asymptotically stable for all values of parameters in the Lyapunov sense.

A.6. Proof of Proposition 2

Assuming $V \neq 0$ and $S = 0$, equilibrium for V is satisfied if

$$V\left(p\Omega(x) - \frac{\varepsilon}{\alpha(1-\omega)}\right) = 0 \Longleftrightarrow p\Omega(x) = \frac{\varepsilon}{\alpha(1-\omega)}, \tag{46}$$

which automatically introduces restriction $\alpha > \varepsilon/(1-\omega)$ since $p \leq 1$ and $\Omega(x) \leq 1$ and we only have $p\Omega(x) = 1$ for $p = 1$ and $V = D = S = 0$, which is biologically impossible. From the equilibrium equation for D, and taking into account equilibrium condition for V, one gets

$$D(V) = \frac{\alpha\omega}{\alpha(1-\omega) - \gamma} V > 0 \Longleftrightarrow \alpha(1-\omega) > \gamma. \tag{47}$$

Thus, in order to obtain biologically meaningful solution values, by virtue of the former considerations, we must have

$$\alpha(1-\omega) > \max\{\varepsilon, \gamma\}. \tag{48}$$

From (46), using expressions for D and p as functions of V given, respectively, by (8) and (47) and after some trivial algebraic manipulations, one gets

$$\varepsilon\kappa\frac{\alpha-\gamma}{\alpha(1-\omega)-\gamma} V^2 - \varepsilon\kappa\left(1 - \frac{\varepsilon}{\alpha(1-\omega)}\right) V + \frac{\varepsilon^2\varepsilon_p}{\alpha(1-\omega)} = 0, \tag{49}$$

which gives rise to a 2nd-degree polynomial in variable V and real coefficients $q_1(V) = T_2V^2 + T_1V + T_0$. Coefficients are labeled as follows:

$$T_2 = \frac{\varepsilon\kappa(\alpha-\gamma)}{\alpha(1-\omega)-\gamma}, \qquad T_1 = -\kappa\varepsilon\left(1 - \frac{\varepsilon}{\alpha(1-\omega)}\right), \qquad T_0 = \frac{\varepsilon_p\varepsilon^2}{\alpha(1-\omega)}. \tag{50}$$

By the Fundamental Theorem of Algebra, $q_1(V)$ has exactly two roots in $\mathbb{C}$. From condition (48), we get $\alpha > \gamma$ since $1 - \omega < 1$ and thus, $T_2 > 0$. We also have $T_0 > 0$. Again, condition (48) leads to $T_1 < 0$. By the Descartes' rule of signs, since there are exactly two changes of sign in the coefficients of $q_1(V)$, it contains either 2 or 0 real and positive roots. Defining the discriminant of $q_1(V)$ as $\Delta = T_1^2 - 4T_2T_0$, we distinguish cases below:

(a) If $\Delta > 0$, since $q_1(-V)$ is a second degree polynomial with real and positive coefficients, the number of negative roots of $q_1(V)$ is zero by virtue of the Descartes' rule of signs. Then, $\Delta > 0$ necessarily leads to the existence of two real and positive roots for $q_1(V)$.

(b) If $\Delta = 0$, then

$$V = \frac{-T_1}{2T_2} > 0, \tag{51}$$

which is a real and positive root with multiplicity 2.

Then, cases (a) and (b) give, at most, two real and positive roots V_1 of $q_1(V)$. For each of these roots, there exist values of p and D given, respectively, by (8) and (47).

A.7. Proof of Proposition 3

Assuming $S_2 \neq 0$, the equilibrium equation $\dot{S} = 0$ reads

$$S_2\left(\beta p_2 \Omega(x_2) - \varepsilon\right) = 0, \tag{52}$$

where p_2 is given by (8) according to the equilibrium equation for p and $x_2 = (V_2, S_2, D_2)$. This equation leads necessarily to condition $p_2\Omega(x_2) = \varepsilon/\beta$. By substituting this expression in the equilibrium equation $\dot{V} = 0$,

$$V_2\left(\alpha(1-\omega)\frac{\varepsilon}{\beta} - \varepsilon\right) = 0.$$

Since $V_2 \neq 0$, this equation is only fulfilled for $\alpha(1-\omega) = \beta$. In particular, for $\alpha(1-\omega) \neq \beta$ there are no coexistence equilibrium points. Assuming both conditions, the equilibrium equation $\dot{D} = 0$ reads

$$\omega\alpha V_2 = (\beta-\gamma)D_2 \Longrightarrow D_2(V_2) = \frac{\omega\alpha}{\beta-\gamma} V_2 = \frac{\beta\omega}{(\beta-\gamma)(1-\omega)} V_2, \tag{53}$$

since $V_2 \neq 0$ and $\alpha(1-\omega) = \beta$. The expression above is only biologically meaningful if $\beta > \gamma$ and using the expressions $p_2(V_2)$ and $D_2(V_2)$, it follows that

$$\begin{aligned} p_2\Omega(x_2) = \frac{\varepsilon}{\beta} &\Leftrightarrow \left(1 - \frac{\varepsilon_p}{\kappa V_2 + \varepsilon_p}\right)\left(1 - V_2 - \frac{\omega\alpha}{\beta-\gamma} V_2 - S_2\right) = \frac{\varepsilon}{\beta} \\ &\Leftrightarrow -\kappa\left(1 + \frac{\omega\alpha}{\beta-\gamma}\right) V_2^2 + \kappa\left(1 - S_2 - \frac{\varepsilon}{\beta}\right) V_2 - \frac{\varepsilon\varepsilon_p}{\beta} = q_2(V_2) = 0. \end{aligned} \tag{54}$$

Therefore, in order for $V_2 \in (0, 1]$ to be biologically meaningful, it must be a root of the polynomial $q_2(V_2)$ defined above. The discriminant Δ_2 of $q_2(V_2)$ is given by:

$$\Delta_2 = \kappa^2\left(1 - S_2 - \frac{\varepsilon}{\beta}\right)^2 - 4\kappa\left(1 + \frac{\alpha\omega}{\beta-\gamma}\right)\frac{\varepsilon\varepsilon_p}{\beta}.$$

Condition $\Delta_2 \geq 0$ provides real solutions for the roots of polynomial $q_2(V_2)$. Then, by solving this inequality in terms of S_2, we have $\Delta_2 \geq 0$ if and only if

$$\begin{aligned} S_2 \in I = &\left(-\infty, 1 - \frac{\varepsilon}{\beta} - 2\sqrt{\frac{\varepsilon\varepsilon_p}{\kappa\beta}\left(1 + \frac{\alpha\omega}{\beta-\gamma}\right)}\right] \\ &\cup \left[1 - \frac{\varepsilon}{\beta} + 2\sqrt{\frac{\varepsilon\varepsilon_p}{\kappa\beta}\left(1 + \frac{\alpha\omega}{\beta-\gamma}\right)}, +\infty\right). \end{aligned}$$

The value of S_2 obtained will be biologically meaningful if and only if $S_2 \in I \cap (0, 1)$. Then, for each value of $S_2 \in I \cap (0, 1)$, the corresponding values of $V_2(S_2)$ are given by the roots of $q_2(V_2)$ in the interval $(0, 1)$. For each of the biologically meaningful values of $V_2(S_2)$, the corresponding values of $D_2(S_2)$ and $p_2(S_2)$ are obtained according to their respective expressions. Then, coexistence equilibrium points are given by the 1-parametric family

$$\mathcal{E} := \{(V_2, S_2, D_2, p_2) = (V_2(S_2), S_2, D_2(S_2), p_2(S_2)) \in \mathcal{U}$$

$$\Big| \; S_2 \in I \cap (0,1),\ q_2(V_2) = 0 \Big\},$$

which corresponds to those values of (V_2, S_2) belonging to the conic (54) that fall into $\mathring{\mathcal{U}}$.

A.8. Proof of Proposition 4

We define the following function:

$$H\,(V(t), D(t)) = D(t) - \frac{\beta\omega}{(\beta-\gamma)(1-\omega)} V(t). \tag{55}$$

Then the surface we want to prove to be invariant is given by $H(V(t), D(t)) = 0$. Using Eqs. (1) and (3), we have:

$$\begin{aligned}\frac{dH(V(t),D(t))}{dt} &= \frac{\partial H}{\partial V}\frac{dV}{dt} + \frac{\partial H}{\partial D}\frac{dD}{dt} = -\frac{\beta\omega}{(\beta-\gamma)(1-\omega)}\dot{V} + \dot{D} \\ &= (\alpha\omega V + \gamma D) p\,\Omega(x) - \varepsilon D - \frac{\beta\omega}{(\beta-\gamma)(1-\omega)}\left(\alpha(1-\omega)V p\,\Omega(x) - \varepsilon V\right).\end{aligned}$$

Evaluating the expression above in the surface $H(V(t), D(t)) = 0$, we obtain:

$$\begin{aligned}\frac{dH(V(t),D(t))}{dt} &= \left(\alpha\omega V + \gamma\frac{\beta\omega}{(\beta-\gamma)(1-\omega)}V\right) p\,\Omega(x) - \varepsilon\frac{\beta\omega}{(\beta-\gamma)(1-\omega)}V \\ &\quad - \frac{\beta\omega}{(\beta-\gamma)(1-\omega)}\alpha(1-\omega)V p\,\Omega(x) + \varepsilon\frac{\beta\omega}{(\beta-\gamma)(1-\omega)}V \\ &= p\,\Omega(x)V\left(\alpha\omega + \frac{\beta\omega\gamma}{(\beta-\gamma)(1-\omega)} - \frac{\beta\omega\alpha(1-\omega)}{(\beta-\gamma)(1-\omega)}\right) \\ &= \frac{p\,\Omega(x)V}{(\beta-\gamma)(1-\omega)}\left(\beta\omega\alpha(1-\omega) - \gamma\omega\alpha(1-\omega) + \beta\omega\gamma - \beta\omega\alpha(1-\omega)\right) \\ &= 0,\end{aligned}$$

where the last equality follows from hypothesis $\alpha(1-\omega) = \beta$. Therefore, $H(V(t), D(t)) = 0$ is invariant for (1)–(4).

A.9. Proof of Proposition 5

Assuming $\alpha(1-\omega) = \beta$, Eqs. (1) and (2) read, respectively, as:

$$\dot{V} = \alpha(1-\omega)V\left(p\,\Omega(x) - \frac{\varepsilon}{\alpha(1-\omega)}\right)$$
$$\text{and} \quad \dot{S} = \alpha(1-\omega)S\left(p\,\Omega(x) - \frac{\varepsilon}{\alpha(1-\omega)}\right), \tag{56}$$

and therefore, assuming $V \neq 0$, one has

$$\dot{S}V - S\dot{V} = 0 \iff \frac{\dot{S}V - S\dot{V}}{V^2} = 0 \iff \frac{d}{dt}\left(\frac{S}{V}\right) = 0,$$

which provides the condition for $S(t)/V(t)$ to be a first integral.

Appendix B. The global bifurcation

B.1. Proof of Lemma 6

From Proposition 2 we know that

$$p_1 = p_1(V_1) = 1 - \frac{\varepsilon_p}{\kappa V_1 + \varepsilon_p}.$$

Since equilibrium points Q_1 satisfy $p\,\Omega(x) = \varepsilon/(\alpha(1-\omega))$, we can express the value of D_1 as

$$D_1(V_1) = 1 - V_1 - \frac{\varepsilon(\kappa V_1 + \varepsilon_p)}{\kappa\alpha V_1(1-\omega)}.$$

Substituting these values into $p\Omega(x)$ we get

$$p\Omega(x)\Big|_{Q_1} = \left(1 - \frac{\varepsilon_p}{\kappa V_1 + \varepsilon_p}\right)\left(\frac{\varepsilon(\kappa V_1 + \varepsilon_p)}{\alpha\kappa V_1(1-\omega)}\right) = \frac{\varepsilon}{\alpha(1-\omega)}.$$

B.2. Proof of Proposition 6

Since system (1)–(4) is analytic, $\mathcal{U}$ is compact and positively invariant by the flow and for $\mu \neq 0$ there are no periodic orbits, equilibrium points exists in the interior $\mathring{\mathcal{U}}$ and numerical evidence discards the existence of invariant torus or quasi-periodic orbits; the only possibility for the ω-limit set of $\varphi(t, y_0)$ is to be equilibrium point on $\{S = 0\}$. By *reductio ad absurdum*, assume $\omega(\varphi) = Q_1$. From Lemma 6 we have:

$$\lim_{t\to+\infty} p\Omega(x)\Big|_{(V,S,D,p)=\varphi(t,y_0)} = \frac{\varepsilon}{\alpha(1-\omega)} > \frac{\varepsilon}{\beta}, \tag{57}$$

where the last inequality follows from condition $\mu < 0$. Therefore, there exists $+\infty > t_1 > 0$ such that

$$p\Omega(x)\Big|_{(V,S,D,p)=\varphi(t,y_0)} > \frac{\varepsilon}{\beta}, \quad \forall t > t_1. \tag{58}$$

Consequently, variable $S(t)$ in $\varphi(t, y_0)$ satisfies

$$\dot{S}(t) = \beta S(t)\left(p\Omega(x) - \frac{\varepsilon}{\beta}\right) > 0, \quad \forall t > t_1, \tag{59}$$

that is to say, $S(t)$ is strictly increasing within interval $(t_1, +\infty)$, which contradicts the fact that $\omega(\varphi) = Q_1$. Notice that $S(t_1) \neq 0$ since $S = 0$ is an invariant manifold and we cannot reach it in finite time for initial conditions in $\mathring{\mathcal{U}}$. Thus, necessarily $\omega(\varphi) = Q_0$.

B.3. Proof of Lemma 7

Assume $\mu < 0$ and, consequently, $\alpha < \alpha^*$. Then, for $\tau_0 < t < \tau_1$, we have:

$$\begin{aligned}\frac{\varepsilon}{\beta} < p\Omega(x) < \frac{\varepsilon}{\alpha(1-\omega)} &\iff 0 < p\Omega(x) - \frac{\varepsilon}{\beta} < \frac{\varepsilon}{\alpha(1-\omega)} - \frac{\varepsilon}{\beta} = \frac{\varepsilon}{\alpha\beta}(\alpha^* - \alpha) \\ &\iff 0 < \beta\left(p\Omega(x) - \frac{\varepsilon}{\beta}\right) < \frac{\varepsilon}{\alpha}(\alpha^* - \alpha) \\ &\iff 0 < \frac{\dot{S}}{S} < \frac{\varepsilon}{\alpha}(\alpha^* - \alpha).\end{aligned}$$

Since $S > 0$ in $\mathcal{U}$, we need $\dot{S} > 0$ in order for the last inequality to be fulfilled. Therefore, for $\tau_0 < t < \tau_1$, $S(t)$ is monotonous increasing and for $t > \tau_1$, according to definition of τ_1, $p\Omega(x) < \varepsilon/\beta$. In this case,

$$p\Omega(x) < \frac{\varepsilon}{\beta} \iff \beta\left(p\Omega(x) - \frac{\varepsilon}{\beta}\right) < 0 \iff \frac{\dot{S}}{S} < 0.$$

By the same argument as above, we need $\dot{S} < 0$ and thus $S(t)$ is monotonous decreasing for $t > \tau_1$. Then necessarily, $S(t)$ must have a local maximum at $t = \tau_1$.

B.4. Proof of Proposition 7

Since $\mu < 0$, we have $\alpha < \alpha^*$. Then, for all $\tau_0 < t < \tau_1$, we have

$$\begin{aligned}\frac{\varepsilon}{\beta} < p\Omega(x) < \frac{\varepsilon}{\alpha(1-\omega)} &\iff 0 < p\Omega(x) - \frac{\varepsilon}{\beta} < \frac{\varepsilon}{\alpha(1-\omega)} - \frac{\varepsilon}{\beta} = \frac{\varepsilon}{\alpha\beta}(\alpha^* - \alpha) \\ &\iff 0 < \beta\left(p\Omega(x) - \frac{\varepsilon}{\beta}\right) < \frac{\varepsilon}{\alpha}(\alpha^* - \alpha) \\ &\iff 0 < \frac{\dot{S}}{S} < \frac{\varepsilon}{\alpha}(\alpha^* - \alpha).\end{aligned}$$

Integrating the expression above in the interval (τ_0, τ_1), we get:

$$0 < \int_{\tau_0}^{\tau_1}\frac{\dot{S}}{S}dt < \frac{\varepsilon}{\alpha}(\alpha^* - \alpha)\int_{\tau_0}^{\tau_1} dt \iff 0 < \log\left(\frac{S(\tau_1)}{S(\tau_0)}\right) < \frac{\varepsilon}{\alpha}(\alpha^* - \alpha)(\tau_1 - \tau_0). \tag{60}$$

Denoting by $S_1 = S(\tau_1)$ and $S_0 = S(\tau_0)$, we have $S_1 > S_0 > 0$. Analogously, for $t \in (\tau_0, \tau_1)$, we can reconstruct the evolution equation for V and integrating the resulting expression in the inequality, we get:

$$0 < \log\left(\frac{V(\tau_0)}{V(\tau_1)}\right) < \frac{\varepsilon}{\alpha^*}(\alpha^* - \alpha)(\tau_1 - \tau_0), \tag{61}$$

where we again denote $V_0 = V(\tau_0)$ and $V_1 = V(\tau_1)$ that satisfy $V_0 > V_1 > 0$. Then, from inequalities (60) and (61), we obtain, respectively:

$$\tau_1 - \tau_0 > \frac{\alpha}{\varepsilon}\frac{1}{\alpha^* - \alpha}\log\left(\frac{S_1}{S_0}\right),$$
$$\tau_1 - \tau_0 > \frac{\alpha^*}{\varepsilon}\frac{1}{\alpha^* - \alpha}\log\left(\frac{V_0}{V_1}\right) > \frac{\alpha}{\varepsilon}\frac{1}{\alpha^* - \alpha}\log\left(\frac{V_0}{V_1}\right).$$

Defining now

$$\tilde{K} := \max\left\{\log\left(\frac{V_0}{V_1}\right), \log\left(\frac{S_1}{S_0}\right)\right\}, \tag{62}$$

which does not depend on μ, we get our result proved taking into account that $|\mu| = \alpha^* - \alpha$:

$$\tau_1 - \tau_0 > \frac{\tilde{K}\alpha}{\varepsilon}\frac{1}{|\mu|}. \tag{63}$$

B.5. Proof of Proposition 8

Let us define

$$\delta_1 = \frac{\varepsilon}{\beta} \quad \text{and} \quad \delta_2 = \frac{\varepsilon}{\alpha(1-\omega)}. \tag{64}$$

Assuming $Q_1 = (V_1, 0, D_1, p_1)$ as the ω-limit of an orbit $\varphi(t, y_0)$, there exists $\xi > 0$ arbitrarily small and $t_0(\xi) > 0$ such that, for all $t > t_0$

$$\left|p\Omega(x) - \delta_2\right| < \xi, \tag{65}$$

since Q_1 is found at the intersection between one of the components of $\dot{V} = 0$ nullcline ($p\Omega(x) = \delta_2$) and the invariant subset $S = 0$, according to Lemma 6. Expression (65) follows directly from the definition of ω-limit. Straightforwardly,

$$\delta_2 - \xi < p\Omega(x) < \delta_2 + \xi < \delta_1, \tag{66}$$

and $p\Omega(x)$ gets infinitely confined.

Data availability

No data was used for the research described in the article.

References

[1] Flint J, Racaniello VR, Rall GF, Hatziioannou T, Skalka AM. Principles of virology. Molecular biology, vol. 1, 2020.

[2] Duffy S, Shackelton LA, Holmes EC. Rates of evolutionary change in viruses: patterns and determinants. Nat Rev Genet 2008;9:267–76. http://dx.doi.org/10.1038/nrg2323.

[3] Ferrer-Orta C, Arias A, Escarmís C, Verdaguer N. A comparison of viral rna-dependent rna polymerases. Curr Opin Struct Biol 2008;16:27–34. http://dx.doi.org/10.1016/j.sbi.2005.12.002.

[4] Sanjuán Rafael, Nebot Miguel R, Chirico Nicola, Mansky Louis M, Belshaw Robert. Viral mutation rates. J Virol 2010;84(19):9733–48. http://dx.doi.org/10.1128/jvi.00694-10.

[5] González Aparicio LJ, López CB. Selection of nonstandard viral genomes during the evolution of rna viruses: A virus survival strategy or a pesky inconvenience? Adv Virus Res 2024;119(2):39–61. http://dx.doi.org/10.1016/bs.aivir.2024.05.002.

[6] Vignuzzi Marco, López Carolina. Defective viral genomes are key drivers of the virus–host interaction. Nat Microbiol 2019;4:1. http://dx.doi.org/10.1038/s41564-019-0465-y.

[7] Huang Alice S, Baltimore David. Defective viral particles and viral disease processes. Nature 1970;226:325–7. http://dx.doi.org/10.1038/226325a0.

[8] Palukaitis Peter. Satellite rnas and satellite viruses. Mol Plant Microbe Interact 2016;29(3):181–6. http://dx.doi.org/10.1094/MPMI-10-15-0232-FI, PMID: 26551994.

[9] Simon Anne E, Roossinck Marilyn J, Havelda Zoltán. Plant virus satellite and defective interfering rnas: new paradigms for a new century. Annu Rev Phytopathol 2004;42(volume 42 2004):415–37. http://dx.doi.org/10.1146/annurev.phyto.42.040803.140402.

[10] Badar Uzma, Venkataraman Srividhya, AbouHaidar Mounir, Hefferon Kathleen. Molecular interactions of plant viral satellites. Virus Genes 2021;57(1):1–22. http://dx.doi.org/10.1007/s11262-020-01806-9.

[11] Schmitt Manfred J, Breinig Frank. The viral killer system in yeast: from molecular biology to application. FEMS Microbiol Rev 2002;26(3):257–76. http://dx.doi.org/10.1111/j.1574-6976.2002.tb00614.x.

[12] Ribière Magali, Olivier Violaine, Blanchard Philippe. Chronic bee paralysis: A disease and a virus like no other? J Invertebr Pathol 2009;103 Suppl 1:S120–31. http://dx.doi.org/10.1016/j.jip.2009.06.013.

[13] Krupovic M, Kuhn JH, Fisher MG. A classification system for virophages and satellite virus. Arch Virol 2016;161:233–47. http://dx.doi.org/10.1007/s00705-015-2622-9.

[14] Gal-On Amit, Kaplan Igor, Palukaitis Peter. Differential effects of satellite rna on the accumulation of cucumber mosaic virus rnas and their encoded proteins in tobacco vs zucchini squash with two strains of cmv helper virus. Virology 1995;208(1):58–66. http://dx.doi.org/10.1006/viro.1995.1129.

[15] Roux Laurent, Simon Anne, Holland John. Effects of defective interfering viruses on virus replication and pathogenesis in vitro and in vivo. Adv Virus Res 1991;40:181–211. http://dx.doi.org/10.1016/S0065-3527(08)60279-1.

[16] Giersch Katja, Helbig Martina, Volz Tassilo, Allweiss Lena, Mancke Lida V, Lohse Ansgar W, et al. Persistent Hepatitis D virus mono-infection in humanized mice is efficiently converted by Hepatitis B virus to a productive co-infection. J Hepatol 2014;60(3):538–44. http://dx.doi.org/10.1016/j.jhep.2013.11.010.

[17] Mentha N, Clément S, Negro F, Alfaiate D. A review on Hepatitis D: From virology to new therapies. J Adv Res 2019;17:3–15. http://dx.doi.org/10.1016/j.jare.2019.03.009, Special Issue on Celebrating JAR-1st IF.

[18] Rizzetto M, Ponzetto A, Bonino F, Smedile A. Viral hepatitis and liver disease. 1988.

[19] Miao Zhijiang, Zhang Shaoshi, Ou Xumin, Li Shan, Ma Zhongren, Wang Wenshi, et al. Estimating the Global Prevalence, Disease Progression, and Clinical Outcome of Hepatitis Delta Virus Infection. J Infect Dis 2019;221(10):1677–87. http://dx.doi.org/10.1093/infdis/jiz633.

[20] Tomás Lázaro J, Albó Ariadna, Alarcón Tomás, Elena Santiago F, Sardanyés Josep. No two without three: Modeling dynamics of the trio rna virus-defective interfering genomes-satellite rnas. Commun Nonlinear Sci Numer Simul 2024;133:107987. http://dx.doi.org/10.1016/j.cnsns.2024.107987.

[21] Rampersad Sephra, Tennant Paula. Chapter 3 - replication and expression strategies of viruses. In: Tennant Paula, Fermin Gustavo, Foster Jerome E, editors. Viruses. Academic Press; 2018, p. 55–82.

[22] Sardanyés Josep, Arderiu Andreu, Elena Santiago F, Alarcón Tomás. Noise-induced bistability in the quasi-neutral coexistence of viral rnas under different replication modes. J R Soc Interface 2018;15(142):20180129. http://dx.doi.org/10.1098/rsif.2018.0129.

[23] Muñoz-Sánchez Juan C, Tomás Lázaro J, Hillung Julia, Olmo-Uceda María J, Sardanyés Josep, Elena Santiago F. Quasineutral multistability in an epidemiological-like model for defective-helper betacoronavirus infection in cell cultures. Appl Math Model 2025;137:115673. http://dx.doi.org/10.1016/j.apm.2024.115673.

[24] Parsons Todd L, Quince Christopher. Fixation in haploid populations exhibiting density dependence II: The quasi-neutral case. Theor Popul Biol 2007;72(4):468–79. http://dx.doi.org/10.1016/j.tpb.2007.04.002.

[25] Parsons Todd L, Quince Christopher, Plotkin Joshua B. Absorption and fixation times for neutral and quasi-neutral populations with density dependence. Theor Popul Biol 2008;74(4):302–10. http://dx.doi.org/10.1016/j.tpb.2008.09.001.

[26] Lorraine Heisler I, Curtsinger James W. Dynamics of sexual selection in diploid populations. Evolution 1990;44(5):1164–76. http://dx.doi.org/10.1111/j.1558-5646.1990.tb05223.x.

[27] Greenspoon Philip B, Otto Sarah P. Evolution by fisherian sexual selection in diploids. Evolution 2009;63(4):1076–83. http://dx.doi.org/10.1111/j.1558-5646.2008.00606.x.

[28] Fontich Ernest, Guillamon Antoni, Tomás Lázaro J, Alarcón Tomás, Vidiella Blai, Sardanyés Josep. Critical slowing down close to a global bifurcation of a curve of quasi-neutral equilibria. Commun Nonlinear Sci Numer Simul 2022;104:106032. http://dx.doi.org/10.1016/j.cnsns.2021.106032.

[29] Lin Yen Ting, Kim Hyejin, Doering Charles. Features of fast living: On the weak selection for longevity in degenerate birth–death processes. J Stat Phys 2012;148:646–62. http://dx.doi.org/10.1007/s10955-012-0479-9.

[30] Farkas M. Zip bifurcation in a competition model. Nonlinear Anal Theory Methods Appl 1984;8(11):1295–309. http://dx.doi.org/10.1016/0362-546X(84)90017-8.

[31] Wiggins Stephen. Normally hyperolic invariant manifolds in dynamical systems. 1994.

[32] Fiedler Bernold, Liebscher Stefan, Alexander JC. Generic hopf bifurcation from lines of equilibria without parameters. I. Theory. J Differential Equations 2000;(167):16–35. http://dx.doi.org/10.1006/jdeq.2000.3779.

[33] Fiedler Bernold, Liebscher Stefan. Bifurcations without parameters: Some ode and pde examples. 2002.

[34] Sun Mengfeng, Lou Yijun, Fu Xinchu. Analysis of equilibria and connecting orbits in a nonlinear viral infection model. SIAM J Appl Dyn Syst 2024;23:1272–312. http://dx.doi.org/10.1137/23M1578115.

[35] Strogatz Steven H, Westervelt Robert M. Predicted power laws for delayed switching of charge-density waves. Phys Rev B 1989;40:10501–8. http://dx.doi.org/10.1103/PhysRevB.40.10501.

[36] Sardanyés Josep, Solé Ricard V. Ghosts in the origins of life? Int J Bifurc Chaos Appl Sci Eng 2006;16(09):2761–5. http://dx.doi.org/10.1142/S0218127406016446.

[37] Sardanyés Josep, Solé Ricard V. The role of cooperation and parasites in non-linear replicator delayed extinctions. Chaos Solit Fractals 2007;31(5):1279–96. http://dx.doi.org/10.1016/j.chaos.2006.04.029.

[38] Sardanyés Josep, Raich Carles, Alarcon Tomas. Noise-induced stabilization of saddle–node ghosts. New J Phys 2020;22:093064. http://dx.doi.org/10.1088/1367-2630/abb549.

[39] Koch Daniel, Nandan Akhilesh, Ramesan Gayathri, Tyukin Ivan, Gorban Alexander, Koseska Aneta. Ghost channels and ghost cycles guiding long transients in dynamical systems. Phys Rev Lett 2024;133:047202. http://dx.doi.org/10.1103/PhysRevLett.133.047202.

[40] Thorne Lucy G, Goodfellow Ian G. Norovirus gene expression and replication. J Gen Virol 2014;95:278–91. http://dx.doi.org/10.1099/vir.0.059634-0.

[41] Raney Kevin D, Sharma Suresh D, Moustafa Ibrahim M, Cameron Craig E. Hepatitis C virus non-structural protein 3 (hcv ns3): A multifunctional antiviral target*. J Biol Chem 2010;285(30):22725–31. http://dx.doi.org/10.1074/jbc.R110.125294.

[42] Takeda K, Komano J. Cellular nucleotide metabolism regulates Hepatitis C virus replication. Sci Rep 2018;8:5956.

[43] Kim SS, Sze L, Liu CM. Host factors essential for rna virus replication. J Gen Virol 2020;101:443–51.

[44] Romero-Brey Inés, Bartenschlager Ralf. Membranous replication factories induced by plus-strand rna viruses. Viruses 2014;6(7):2826–57. http://dx.doi.org/10.3390/v6072826.

[45] Martínez Fernando, Sardanyés Josep, Elena Santiago F, Daròs José-Antonio. Dynamics of a plant RNA virus intracellular accumulation: Stamping machine vs. Geometric replication. Genetics 2011;188(3):637–46. http://dx.doi.org/10.1534/genetics.111.129114.

[46] Dimmock Nigel J, Easton Andrew J. Defective interfering influenza virus rnas: Time to reevaluate their clinical potential as broad-spectrum antivirals? J Virol 2014;88(10):5217–27. http://dx.doi.org/10.1128/jvi.03193-13.

[47] Cave DR, Hendrickson FM, Huang AS. Defective interfering virus particles modulate virulence. J Virol 1985;55(2):366–73. http://dx.doi.org/10.1128/jvi.55.2.366-373.1985.

[48] Li XH, Heaton LA, Morris TJ, Simon AE. Turnip crinkle virus defective interfering rnas intensify viral symptoms and are generated de novo. Proc Natl Acad Sci USA 1989;86(23):9173–7. http://dx.doi.org/10.1073/pnas.86.23.9173.

[49] Thompson Kristen, Yin John. Population dynamics of an rna virus and its defective interfering particles in passage cultures. Virol J 2010;7:257. http://dx.doi.org/10.1186/1743-422X-7-257.

[50] Timm Collin, Akpinar Fulya, Yin John. Quantitative characterization of defective virus emergence by deep sequencing. J Virol 2014;88(5):2623–32. http://dx.doi.org/10.1128/jvi.02675-13.

[51] Jaworski Elizabeth, Routh Andrew. Parallel clickseq and nanopore sequencing elucidates the rapid evolution of defective-interfering rnas in flock house virus. PLoS Pathog 2017;13(5):1–31. http://dx.doi.org/10.1371/journal.ppat.1006365.

[52] Gribble Jennifer, Stevens Laura J, Agostini Maria L, Anderson-Daniels Jordan, Chappell James D, Lu Xiaotao, et al. The coronavirus proofreading exoribonuclease mediates extensive viral recombination. PLoS Pathog 2021;17(1):1–28. http://dx.doi.org/10.1371/journal.ppat.1009226.

[53] Hillung Julia, Olmo-Uceda María J, Muñoz-Sánchez Juan C, Elena Santiago F. Accumulation dynamics of defective genomes during experimental evolution of two betacoronaviruses. Viruses 2024;16(4). http://dx.doi.org/10.3390/v16040644.

[54] Rangel Mauricio, Dolan Patrick, Taguwa Shuhei, Xiao Yinghong, Andino Raul, Frydman Judith. High-resolution mapping reveals the mechanism and contribution of genome insertions and deletions to rna virus evolution. Proc Natl Acad Sci USA 2023;120:e2304667120. http://dx.doi.org/10.1073/pnas.2304667120.

[55] Szathmáry Eörs. Natural selection and dynamical coexistence of defective and complementing virus segments. J Theoret Biol 1992;157(3):383–406. http://dx.doi.org/10.1016/S0022-5193(05)80617-4.

[56] Szathmáry Eörs. Co-operation and defection: Playing the field in virus dynamics. J Theoret Biol 1993;165(3):341–56. http://dx.doi.org/10.1006/jtbi.1993.1193.

[57] Kirkwood TB, Bangham CR. Cycles, chaos, and evolution in virus cultures: a model of defective interfering particles. Proc Natl Acad Sci USA 1994;91(18):8685–9. http://dx.doi.org/10.1073/pnas.91.18.8685.

[58] Frank Steven. Within-host spatial dynamics of viruses and defective interfering particles. J Theoret Biol 2000;206:279–90. http://dx.doi.org/10.1006/jtbi.2000.2120.

[59] Sardanyés Josep, Elena Santiago F. Error threshold in rna quasispecies models with complementation. J Theoret Biol 2010;265(3):278–86. http://dx.doi.org/10.1016/j.jtbi.2010.05.018.

[60] Zwart Mark, Pijlman Gorben, Sardanyés Josep, Duarte Jorge, Januário Cristina, Elena Santiago. Complex dynamics of defective interfering baculoviruses during serial passage in insect cells. J Biol Phys 2013;39. http://dx.doi.org/10.1007/s10867-013-9317-9.

[61] Chaturvedi Sonali, Vasen Gustavo, Pablo Michael, Chen Xinyue, Beutler Nathan, Kumar Arjun, et al. Identification of a therapeutic interfering particle—a single-dose sars-cov-2 antiviral intervention with a high barrier to resistance. Cell 2021;184(25):6022–36.e18. http://dx.doi.org/10.1016/j.cell.2021.11.004.

[62] Kogan Oleg, Khasin Michael, Meerson Baruch, Schneider David, Myers Christopher R. Two-strain competition in quasineutral stochastic disease dynamics. Phys Rev E 2014;90:042149. http://dx.doi.org/10.1103/PhysRevE.90.042149.